E11850

Twenty-Seventh Symposium (International) on Combustion/The Combustion Institute, 1998/pp. 2485–2506

i 420304

UNDERSTANDING COMBUSTION PROCESSES THROUGH MICROGRAVITY RESEARCH

PAUL D. RONNEY

Department of Aerospace and Mechanical Engineering
University of Southern California
Los Angeles, CA 90089-1453, USA

A review of research on the effects of gravity on combustion processes is presented, with an emphasis on a discussion of the ways in which reduced-gravity experiments and modeling has led to new understanding. Comparison of time scales shows that the removal of buoyancy-induced convection leads to manifestations of other transport mechanisms, notably radiative heat transfer and diffusional processes such as Lewis number effects. Examples from premixed-gas combustion, non-premixed gas-jet flames, droplet combustion, flame spread over solid and liquid fuels, and other fields are presented. Promising directions for new research are outlined, the most important of which is suggested to be radiative reabsorption effects in weakly burning flames.

Introduction

Gravity influences many combustion processes, particularly due to buoyant convection which affects transport of thermal energy and reactants to and from the chemical reaction zones. Recently, many experimental and theoretical studies of combustion at microgravity (μg) conditions have been conducted. These studies are motivated by the need to assess fire hazards in spacecraft and to enable better understanding of combustion processes at earth gravity (1g) through the elimination of buoyancy [1–4].

This paper discusses how new understanding of combustion processes has been obtained through μg research, rather than providing a comprehensive review of this rapidly changing field. First, comparisons of time scales for various chemical and transport processes in flames, including buoyancy-induced transport, are given. Next, examples of unexpected results and new understandings obtained through μg research are discussed. These findings are then summarized and future research directions are suggested.

Comparison of Time Scales for Premixed-Gas Combustion

To determine the conditions in which gravity can affect flames, the estimated time scales for chemical reaction (t_{chem}), inviscid buoyant convection (t_{inv}), viscous buoyant convection (t_{vis}), conductive heat loss to walls (t_{cond}), and radiant heat loss (t_{rad}) are compared. Premixed laminar flames are considered first because of their simplicity. Subsequent sections introduce time scales for other flames.

The chemical time scale is (see Nomenclature) $t_{chem} \approx \delta/S_L$ where $\delta = \alpha/S_L$, thus $t_{chem} \approx \alpha/S_L^2$. The convective transport time scale is d/U, where d is a characteristic flow length scale, $U \approx (gd(\Delta\rho/\rho))^{1/2}$ is the buoyant convection velocity, and $\Delta\rho$ the density change across the flame. Because $\Delta\rho/\rho \approx 1$ for flames, $t_{inv} \approx d/(gd)^{1/2} = (d/g)^{1/2}$. For inviscid flow, d is determined by the apparatus dimensions, for example the burner or tube diameter. For viscous flow, d cannot be specified independently; instead $d \approx \nu/U$, thus $U \approx (g\nu)^{1/3}$ and $t_{vis} \approx d/U \approx (\nu/U)/U \approx (\nu/g^2)^{1/3}$ the conduction time scale t_{cond} is the flame front temperature (T_f) divided by the rate of temperature decrease due to conductive loss; thus $t_{cond} = T_f/(dT/dt) \approx T_f/(\rho C_P h(T_f - T_\infty))$; thus $t_{cond} \approx d^2/16\alpha$. Similarly, for optically thin radiation, $t_{rad} \approx T_f/(\Lambda/\rho C_P) \approx \{\gamma/(\gamma - 1)\}\{P/4\sigma a_P(T_f^4 - T_\infty^4)\}$.

Two sets of time scales are shown in Table 1, one for near-stoichiometric hydrocarbon–air flames and one for near-limit flames, both at $P = 1$ atm. For near-stoichiometric flames $S_L \approx 0.40$ m/s, $T_f \approx 2200$ K, $\alpha \approx \nu$ 1.5×10^{-4} m^2/s and $a_P \approx 0.56$ m^{-1}. For near-limit flames, $S_L \approx 0.02$ m/s, $T_f \approx 1500$ K, $\alpha \approx \nu \approx 1.0 \times 10^{-4}$ m^2/s and $a_P \approx 0.83$ m^{-1}. For both cases $g \approx 9.8$ m/s^2, $\gamma \approx 1.35$, $T_\infty \approx 300$ K and $d \approx 0.05$ m (a typical apparatus dimension.)

Several observations can be made on the basis of these simple estimates:

1. Buoyant convection is unimportant for near-stoichiometric flames because $t_{vis} \gg t_{chem}$ and $t_{inv} \gg t_{chem}$.
2. Buoyant convection strongly influences near-limit flames at 1g because $t_{vis} \leq t_{chem}$ and $t_{inv} \leq t_{chem}$.
3. Radiation effects are unimportant at 1g compared to buoyant convection because $t_{vis} \ll t_{rad}$ and $t_{inv} \ll t_{rad}$.

TABLE 1
Estimates of time scales for stoichiometric and near-limit hydrocarbon-air flames at 1 atm pressure

Time Scale	Stoichiometric Flame	Near-Limit Flame
Chemistgry (t_{chem})	0.00094 s	0.25 s
Buoyant, inviscid (t_{inv})	0.071 s	0.071 s
Buoyant, viscous (t_{vis})	0.012 s	0.010 s
Conduction to tube wall (t_{cond})	0.95 s	1.4 s
Radiation (t_{rad})	0.13 s	0.41 s

4. Radiation effects dominate near-limit flames because $t_{rad} \approx t_{chem}$, but these effects are only observable at reduced gravity because of observation 3.
5. The apparatus size (d) must be larger than about 0.03 m to observe radiation-induced extinction; otherwise, conduction losses exceed radiative losses ($t_{cond} < t_{rad}$).
6. Many radiative loss effects can be studied in drop-towers (test duration 2–10 s), because these times are typically larger than t_{rad}.
7. Because $t_{inv} \sim g^{1/2}$ and $t_{vis} \sim g^{1/3}$, aircraft-based μg experiments at $g \approx 10^{-2}\ g_o$ may not provide sufficiently reduced buoyancy to observe radiative effects.
8. Because $t_{vis} \sim \nu^{1/3} \sim P^{-1/3}$ and $t_{rad} \sim \rho/\Lambda \sim P^1/P^1 \sim P^0$, $t_{vis}/t_{rad} \sim P^{-1/3}$. Thus, t_{rad} is independent of P, but at higher P, buoyancy effects interfere more strongly with radiative effects.
9. A Reynolds number $Re_d \equiv Ud/\nu$ for buoyant flow is estimated as $(gd)^{1/2}d/\nu^2 = Gr_d^{1/2}$, where $Gr_d \equiv gd^3/\nu^2$ is a Grashof number. For $Re_d \geq 10^3$, thus $Gr_d \geq 10^6$, buoyant flow at 1g is generally turbulent, thus, it difficult to obtain steady laminar flames in large systems at 1g.

The implications of these observations are discussed in the following sections. Essentially, any combustion process where t_{chem} or t_{rad} exceeds t_{inv} or t_{vis} may be affected by gravity and is worthy of μg investigation.

Premixed Gas Flames

Flammability Limits

The previous section showed that gravity effects are significant only for mixtures with low S_L, implying mixtures highly diluted with excess fuel, oxidant, or inert gas, but sufficient dilution causes flammability limits. Thus, gravity effects have significant influences on near-limit behavior, which is expected since limits are different for upward, downward, and horizontal propagation [5].

Practically all flammability limit studies show that burning velocity *at the flammability limit* ($S_{L,lim}$) is nonzero. Giovangigli and Smooke [6] have shown that there is no purely chemical flammability limit criterion for planar unstretched flames; without losses, S_L decreases asymptotically to zero as dilution increases. Consequently, loss mechanisms such as those discussed below are needed to explain limit mechanisms. The resulting predictions of $S_{L,lim}$ indicate that $S_{L,lim}$ usually depends only weakly on chemical reaction rate parameters. Thus, limit mechanisms may be inferred by comparing predicted and measured $S_{L,lim}$ without detailed chemical knowledge. The mixture composition at the limit affects $S_{L,lim}$ only weakly through T_f: thus, comparing predicted and measured limit compositions is not especially enlightening; comparisons of $S_{L,lim}$ values is much more useful. Consequently, this discussion emphasizes comparisons of predicted and measured values of $S_{L,lim}$.

For upward propagation, Levy [7] showed that the flame rise speed at the limit ($\approx 0.33(gd)^{1/2}$) is identical to that of an inviscid hot gas bubble. This relation was later verified for a wide range of tube diameters and mixtures [8]. Buckmaster and Mikolaitis [9] showed how this minimum rise speed causes hydrodynamic strain at the flame tip, which causes extinguishment for sufficiently low S_L. The predicted burning velocity of the limit mixture ($S_{L,lim}$) is, after temperature-averaging transport properties:

$$S_{L,lim} = 2.8 \exp\left[\frac{\beta}{4}\left(1 - \frac{1}{Le}\right)\left(1 - \frac{T_\infty}{T_f}\right)\right]\left(\frac{g\alpha^2}{d}\right)^{1/4} \quad (1)$$

The form of equation 1, $S_{L,lim} \sim (g\alpha^2/d)^{1/4}$, can be obtained by setting $t_{inv} = t_{chem}$.

For downward propagation in tubes, centrifuge experiments [10] indicate that $S_{L,lim} \sim g^{1/3}$, independent of Le, which is reasonable since downward-propagating near-limit flames are nearly flat and unstrained. Experiments [11] and numerical simulations [12] suggest extinction results from sinking regions of cooling burned gas near the walls overtaking the flame and blocking it from fresh reactants, although the $g^{1/3}$ scaling was not tested in Refs. [11,12]. The $g^{1/3}$ scaling can be obtained by setting $t_{chem} = t_{vis}$, thus

$$S_{L,lim} \sim (g\alpha)^{1/3} \quad (2)$$

Experiments [8] employing varying diluent gases and pressures confirm the $\alpha^{1/3}$ scaling and lack of dependence on tube size, which, together with the $g^{1/3}$ scaling mentioned above, supports the proposed mechanism.

Both upward- and downward-limit mechanisms indicate that as $g \to 0$, $S_{L,lim} \to 0$, implying arbitrarily

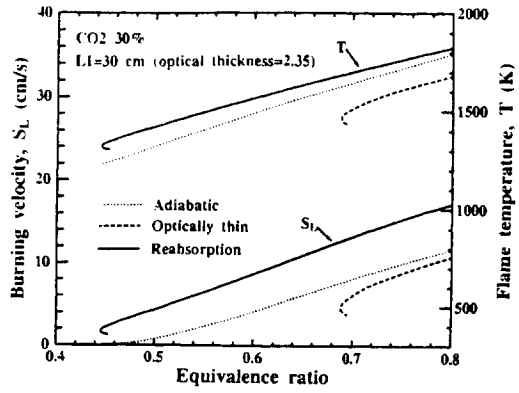

FIG. 1. Predicted values of burning velocity and peak flame temperature in $CH_4 - (0.21\ O_2 + 0.49\ N_2 + 0.30\ CO_2)$ mixtures under adiabatic conditions, with optically thin radiative losses and including reabsorption effects [26].

weak mixtures could burn very slowly. However, conductive or radiative losses prevent arbitrarily weak mixtures from burning even at $g = 0$. Theories that relate flammability limit to heat losses [13–15] predict a minimum T_f below which flame propagation cannot occur because chemical reaction rates are much stronger functions of temperature than heat loss rates (exponential vs. algebraic). Consequently, because dilution decreases T_f, dilution increases the impact of losses, leading to flammability limits. For conductive losses, setting $t_{chem} = t_{cond}$ leads to

$$Pe_{lim} \equiv S_{L,lim} d/\alpha = \text{constant} \qquad (3)$$

with experiments [8,16] and computations [17] indicating $Pe_{lim} \approx 40$. For radiative losses, setting $t_{chem} = t_{rad}$ leads to [18,19]

$$S_{L,lim} = \frac{1}{\rho_\infty C_p} \sqrt{\frac{1.2\beta A \lambda_f}{T_f}} \qquad (4)$$

For lean-limit CH_4–air mixtures at 1 atm, equation 4 yields $S_{L,lim} \approx 0.023$ m/s, similar to detailed numerical model predictions [20,21]. Such small $S_{L,lim}$ are not observed at 1g because of buoyant convection ($t_{inv} < t_{rad}$ and $t_{vis} < t_{rad}$); equations 1 and 2 yield $S_{L,lim} \approx 0.033$ and 0.078 m/s for upward and downward propagation, respectively. At μg, however, predictions of equation 4 compare favorably to experiments in large combustion vessels [19,22] using varying pressures, fuels, and inert gases. Also, similar results were obtained for CH_4–air mixtures at 1 atm in tubes with $d = 0.05$ m [23], suggesting these limits are apparatus-independent. Thus, radiative losses may cause flammability limits when extrinsic losses (conduction, buoyant convection, etc.) are eliminated. In this instance, μg experiments enabled observation of phenomena not observable at 1g.

These radiative effects apply only for optically thin gases (i.e., no reabsorption of emitted radiation), which are inappropriate for large systems, high pressures, or mixtures with strongly absorbing material. With this motivation, μg experiments [24] were conducted using lean CH_4–air mixtures seeded with SiC particles. Because solids emit/absorb as black- or gray-bodies, whereas gases radiate in narrow spectral bands, particle-seeded gases emit/absorb more radiation than particle-free gases. Measurements of propagation rates, pressures and postflame thermal decays showed that, consistent with theoretical predictions [25], at low particle loadings the particles increase radiative loss (optically thin conditions), whereas at higher loadings reabsorption of emitted radiation becomes significant, which decreases net radiative loss and augments conductive heat transport.

Even for gases, computations [26] using detailed statistical narrow-band radiation models show that flammability limits are extended considerably with reabsorption (Fig. 1). With gases, however, two mechanisms lead to flammability limits even with reabsorption. One is the difference in composition between reactants and products; if H_2O or other radiatively active combustion products are absent from the reactants, radiation from these species that is emitted upstream cannot be reabsorbed by the reactants. The second mechanism is that emission spectra are broader at T_f than T_∞; thus, some radiation emitted near the flame front cannot be absorbed by the reactants. Upstream loss occurs via both mechanisms, leading to extinction of weak mixtures. These results suggest that fundamental (domain- and gravity-independent) flammability limits due to radiative losses may exist at μg, but these limits are strongly dependent on emission/absorption spectra of reactant and product gases and their temperature dependence and cannot be predicted using gray-gas or optically-thin model parameters.

Stretched Flames

Premixed gas flames generally are not flat and steady nor do they propagate into quiescent flows. Consequently, flames are subject to "flame stretch," $\Sigma \equiv (1/A)(dA/dt)$ [18], which affects S_L and extinction conditions [18,27]. At 1g, buoyancy imposes flame stretch comparable to t_{inv}^{-1} or t_{vis}^{-1}. At μg, weak flame stretch effects that are insignificant at 1g may dominate. One example is expanding spherical flames for which

$$\Sigma \equiv \frac{1}{A}\frac{dA}{dt} = \frac{1}{4\pi r_f^2}\frac{d}{dt}(4\pi r_f^2) = \frac{2}{r}\frac{dr_f}{dt} \qquad (5)$$

For $Le < 1$, positive stretch increases T_f because the increased chemical enthalpy diffusion to the flame front in the form of scarce reactant exceeds the increased thermal enthalpy loss. Because heat release

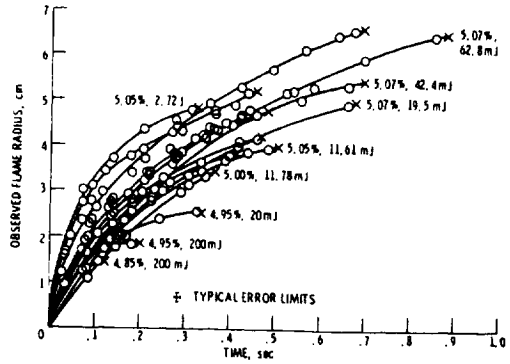

FIG. 2. Characteristics of self-extinguishing flames in CH_4-air mixtures at 1 atm for various mole percent CH_4 and spark ignition energies [112]. The "x" symbols denote extinction.

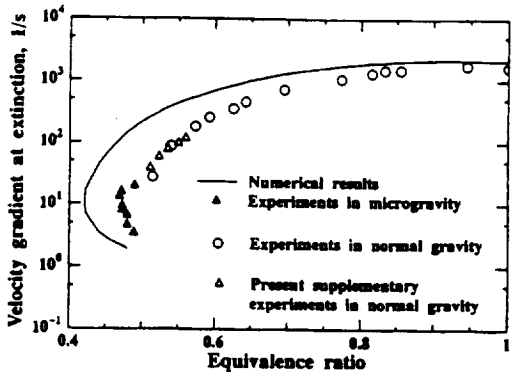

FIG. 3. Measured and predicted extinction strain rates for strained premixed CH_4-air flames at μg [33] showing dual-limit behavior, that is, residence-time limited extinction at high strain rates (upper branch, "strong flames") and radiative loss extinction at low strain rates (lower branch, "weak flames").

reactions have high activation energies, small T_f changes cause large changes in reaction rate and thus S_L. An evolution equation for nonadiabatic expanding spherical flames is given by [28]:

$$\frac{dS}{dR} + S^2 \ln S^2 = \frac{2S}{R} - Q \qquad (6)$$

where $S \equiv (dr_f/dt)/(S_L(\rho_u/\rho_f))$, $R \equiv r_f/(\beta\delta I(Le, \varepsilon))$, $I(Le, \varepsilon)$ is a scaling function ($I > 0$ for $Le < 1$ and $I < 0$ for $Le > 1$) and $Q \equiv \{\beta A(T_f)\delta^2\}/\{\lambda(T_f - T_\infty)\}$. The terms in equation 6 represent unsteadiness, heat release, curvature-induced stretch, and heat loss, respectively. For steady planar flames, equation 6 becomes $S^2 \ln S^2 = -Q$, which exhibits a maximum $Q = 1/e = 0.3678\ldots$ at $S = e^{-1/2}$, which corresponds to $S_{L,lim}$ from equation 4. For $Le < 1$, the curvature effect ($2S/R$) opposes heat loss (Q), allowing mixtures that are nonflammable as plane flames ($Q > 1/e$) to exhibit expanding spherical flames until r_f grows too large and thus the curvature benefit too small. For mixtures just outside the limit, the extinction radius may be very large. Such behavior, termed self-extinguishing flames (SEFs), is observed experimentally [19,22] (Fig. 2) at μg in near-limit mixtures with Le slightly less than unity. (Mixtures with lower Le exhibit diffusive-thermal instabilities or flame balls discussed below.) Equation 6 also predicts, consistent with experimental observations [29], that SEFs cannot occur for $Le > 1$ (thus, $R < 0$) because both curvature and heat loss weaken the flame.

Two experimental observations not predicted by equation 6 are that narrow mixture ranges exhibit both SEFs and normal flames and that the energy release before extinguishment can be orders of magnitude greater than the ignition energy. Such behavior is predicted by computations [30] not subject to scaling limitations of activation energy asymptotics used to derive equation 6. These calculations also show that for small initial r_f, all mixtures exhibit extinguishment, corresponding to nonignition behavior [31]. Thus, in mixtures exhibiting SEFs, flames extinguish at large curvature (small r_f) due to large Σ and at small curvature due to radiative losses. This dual-limit behavior is also exhibited by many other types of flames described later.

Flames in hydrodynamic strain induced by counterflowing round jets are frequently employed to model turbulence-induced flame stretch effects. At steady state, the flame resides at the axial location (y) where the axial velocity (U_y) equals S_L for the given $\Sigma = dU_y/dy$. As Σ increases, U_y increases, thus the flame moves toward the stagnation plane (smaller y) and the burned gas volume (thus radiative loss) decreases. As with curvature-induced stretch, for Le less than/greater than unity, moderate hydrodynamic strain increases/decreases S_L, but for all Le, large strain extinguishes the flame [32]. Consequently, μg experiments [33] in low-Le mixtures (Fig. 3) reveal extinction behavior analogous to spherical flames. For large Σ, the short residence time ($\sim\Sigma^{-1}$) causes extinguishment ($\Sigma^{-1} \approx t_{chem}$) along the "normal flame" branch, analogous to nonignition behavior of spherical flames. In contrast, for low Σ, the residence time and burned gas volume are large; thus, radiative loss is significant ($t_{rad} \approx t_{chem}$), so radiative loss extinguishes the flame along the "weak flame" branch, analogous to SEFs. The optimal Σ ($\approx 13\ s^{-1}$) producing the minimum flammable fuel concentration corresponds to $\Sigma^{-1} = 0.08$ s, which is less than t_{vis} or t_{inv}; thus, the C-shaped response and the entire weak-flame branch cannot be observed at 1g. The optimal Σ is nearly the same for model and experiment, indicating that loss rates are modeled well, but the computed limit

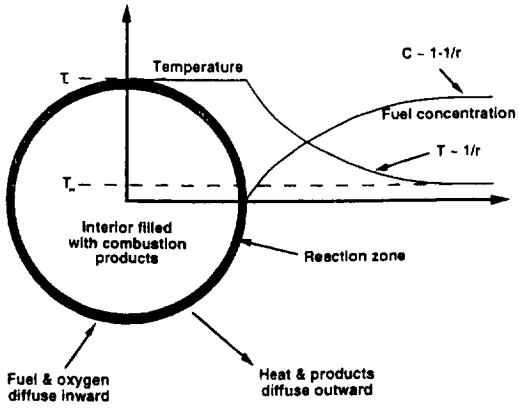

FIG. 4. Schematic diagram of a flame ball, illustrated for the case of fuel-limited combustion at the reaction zone. The oxygen profile is similar to the fuel profile except its concentration is nonzero in the interior of the ball. The combustion product profile is identical to the temperature profile except for a scale factor.

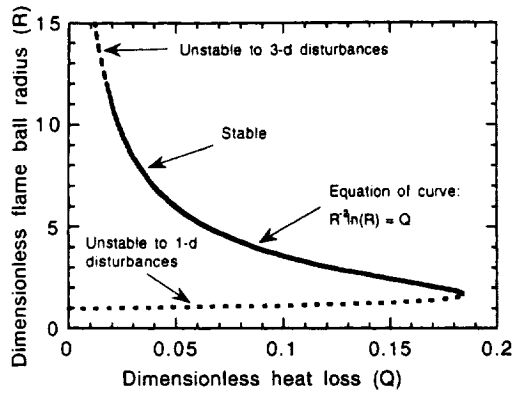

FIG. 5. Predicted effect of heat loss on flame-ball radius and stability properties [42] showing radially unstable (small) flame-ball solution, radially stable (large) flame-ball solution, and three-dimensional instability for large flame balls.

composition is leaner than the experimental limit, suggesting that the chemical mechanism used is inaccurate for weak mixtures. Due to the radiant loss decrease at moderate Σ, the flammability limit extension also occurs for $Le > 1$, though, for sufficiently high Le, no C-shaped response or flammability limit extension occurs [34]. (For spherically expanding flames, no flammability extension occurs for $Le > 1$ because in this case there is no mechanism to reduce radiative loss by flame stretch.)

The combination of nonmonotonic response to Σ plus the reduced radiative loss at larger Σ causes several new extinction branches depending on t_{chem}, t_{rad}, Σ^{-1}, and Le [34,35]. It is uncertain whether these branches are physically observable because they have not been identified experimentally and stability analyses have not been performed.

Flame Balls

Over 50 years ago, Zeldovich [36] showed that the steady mass, energy, and species conservation equations admit solutions corresponding to *stationary* spherical flames, characterized by a flame radius (r_f). Fuel and oxygen diffuse from the ambient mixture inward to the reaction zone while heat and combustion products diffuse outward (Fig. 4). Mass conservation requires that the fluid velocity be zero everywhere. The temperature and species mass fraction profiles have the form $c_1 + c_2/r$, where c_1 and c_2 are constants. Corresponding solutions in planar and cylindrical geometry cannot exist because the solution forms $c_1 + c_2 r$ and $c_1 + c_2 \ln(r)$, respectively, are unbounded as $r \to \infty$. Zeldovich [36] and others [37,38] also showed that flame-ball solutions are *unstable* and thus probably not physically observable, although these solutions are related to flame ignition [37].

Forty years after Zeldovich [36], apparently *stable* flame balls were accidentally discovered in drop-tower experiments using H_2-air mixtures [39] and aircraft-based μg experiments using various low-Le mixtures [40]. The μg environment facilitated spherical symmetry and prevented buoyancy-induced extinction. For mixtures sufficiently far from flammability limits, expanding spherical fronts composed of many individual cells were observed, whereas for more dilute mixtures, cells that formed initially did not split and instead closed up on themselves to form flame balls. (For still more dilute mixtures all flames eventually extinguished.) It was inferred that flame balls can occur in all near-limit low-Le mixtures; however, the short duration of drop-tower experiments and substantial g fluctuations in the aircraft-based μg experiments precluded definite conclusions. Recent space shuttle experiments [41] confirmed that flame balls can exist for at least 500 seconds (the entire experiment duration.)

Zeldovich [36] noted that radiative losses might stabilize flame balls; consequently, after their experimental observation, radiative loss effects on flame balls were analyzed [42]. For moderate loss, two solutions branches are predicted (Fig. 5), a strongly nonadiabatic large-radius branch and a nearly-adiabatic small-radius branch. For sufficiently strong losses, no solutions exist, indicating extinction limits. Stability analyses [42] predict that all small flames are unstable to radial disturbances, and large flames with weak loss (far from flammability limits) are unstable to three-dimensional disturbances. Close to extinction limits, the large-radius branch is stable to both disturbances. These predictions are consistent

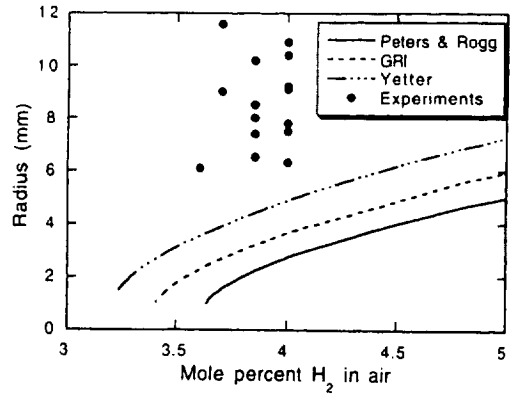

FIG. 6. Comparison of computed flame-ball radii as a function of H_2 mole fraction in H_2-air mixtures for three different H_2–O_2 chemical mechanisms, along with preliminary results from the STS-83 and STS-94 space experiments [45].

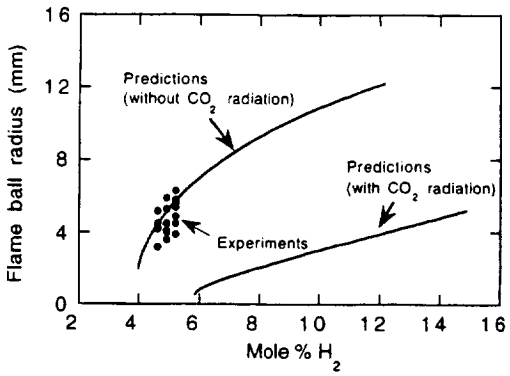

FIG. 7. Computed flame-ball radii as a function of the H_2 mole fraction for steady flame balls in H_2–O_2–CO_2 mixtures with H_2:O_2 = 1:2, for optically thin CO_2 radiation and with CO_2 radiation artificially suppressed (optically thick limit for CO_2 radiation). Preliminary experimental results from the STS-94 mission are also shown (filled circles) [45].

with the observed splitting cellular flames away from limits and stable balls close to limits. For *Le* close to or larger than unity, all flame balls are unstable for any loss magnitude [43], explaining why they are never observed in (for example) CH_4-air mixtures ($Le \approx 0.9$) or C_3H_8-air mixtures ($Le \approx 1.7$).

Numerical predictions of non-adiabatic flame balls employing detailed chemistry, diffusion, and radiation models [44,45] are qualitatively consistent with these experimental and theoretical results. Still, quantitative agreement has been elusive (Fig. 6) for at least two reasons. First, flame-ball properties are very sensitive to the three-body recombination step $H + O_2 + H_2O \rightarrow HO_2 + H_2O$ [45] whose rate varies widely between different published H_2–O_2 reaction mechanisms. The second reason is reabsorption of emitted radiation in mixtures diluted with radiatively active CO_2 or SF_6. An upper bound on self-absorption of diluent radiation ($a_P \rightarrow \infty$) is assessed by neglecting diluent radiation entirely because as $a_P \rightarrow \infty$, radiative loss from the diluent vanishes and no additional heat transport occurs due to radiation. Agreement between predicted and measured flame radii is much better in this case (Fig. 7), strongly suggesting radiation modeling including reabsorption is needed for accurate predictions in these cases.

A key difference between propagating flames and flame balls is that propagating flames have convective-diffusive zones where temperature and concentration approach their ambient values in proportion to $e^{-r/\delta}$, whereas flame balls have purely diffusive zones where the approach is proportional to $1/r$. Plane flames respond on short time scales $t_{chem} = \delta^2/\alpha$, whereas the gradual $1/r$ flame-ball profiles produce properties dominated by the far-field length scale βr_f, and thus diffusion time scales $(\beta r_f)^2/\alpha$ [42], typically 100 s. These scales are relevant to stability and extinction limits because they affect the times for radiant combustion products to diffuse to the far-field and indicate large volumes of gas ($\sim \beta^3 r_f^3$) where radiative loss affects flame balls. Such large scales are confirmed by space experiments [41] and numerical simulations [44,45]. Droplet and candle flames (discussed later), which have quasi-spherical, diffusion-dominated far-fields, exhibit analogous behavior.

Gaseous Non-Premixed Flames

Stretched Flames

Non-premixed flames, where fuel and oxidant are separated before combustion, are affected by stretch differently than are premixed flames. The most significant difference is that the flame position is determined by the location of stoichiometric mixture fraction, dictated by mixing considerations, rather than being determined by balances between S_L and U as in premixed flames. Consequently, non-premixed flames have considerably less freedom of movement. Also, premixed flames have characteristic thicknesses $\delta \sim \alpha/S_L$ unrelated to the flow environment, whereas non-premixed flames have only the diffusion length scale $\delta \sim (\alpha/\Sigma)^{1/2}$. With fixed flame location and δ increasing monotonically with decreasing Σ, non-premixed flames with radiative loss exhibit only simple C-shaped responses to strain (Fig. 8) [46], with a short residence time extinction branch ($t_{chem} > \Sigma^{-1}$) and a radiative loss extinction

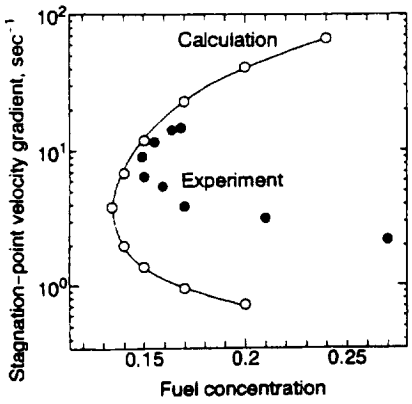

FIG. 8. Measured and predicted extinction strain rates for strained non-premixed N_2-diluted CH_4 versus air counterflow flames at μg [46] showing dual-limit response analogous to premixed flames (Fig. 3).

TABLE 2
Predicted scalings of flame heights (L_f) and residence times (t_{jet}) for non-premixed round-jet and slot-jet flames under momentum-dominated and buoyancy-dominated conditions

Geometry	Flow Mechanism	L_f	t_{jet}
Round-jet	Momentum	$U_o d_o^2/D$	d_o^2/D
Round-jet	Buoyant	$U_o d_o^2/D$	$(U_o d_o^2/gD)^{1/2}$
Slot-jet	Momentum	$U_o d_o^2/D$	d_o^2/D
Slot-jet	Buoyant	$(U_o^4 d_o^4/D^2 g)^{1/3}$	$(U_o^2 d_o^2/g^2 D)^{1/3}$

branch ($t_{rad} < \Sigma^{-1}$) rather than the complicated responses found for premixed flames [34]. The only significant difference in flame structures near the two limits is δ [46], a situation quite unlike premixed flames.

For the radiative extinction branch t_{chem} is still a factor because $t_{rad} \approx \Sigma^{-1}$ results in order unity decreases in flame temperature, thus causing exponentially large decreases in t_{chem}. Even conditions far from extinction at 1g, therefore, may exhibit radiative extinction at μg due to much larger residence times. This mechanism also applies to radiative extinction of other types of non-premixed flames discussed later. It is also somewhat analogous to the lower branch of strained premixed flames (Fig. 3) and the large-radius branch of flame balls (Fig. 5).

The experiments shown in Fig. 8 suggests that no flames exist below some value of Σ, whereas the model predicts flames at arbitrarily low Σ. Similar behavior was seen for premixed flames (Fig. 3). This suggests an additional loss mechanism not considered by the model, probably axial conductive heat losses to the jets or radial conductive loss to inert gases surrounding the reactant streams. This would induce $t_{cond}^{-1} \approx 2.9\ s^{-1}$ if d is the jet spacing (25 mm), or $7.1\ s^{-1}$ if d is the jet diameter (16 mm). Either of these are roughly consistent with the minimum Σ in Fig. 8. Thus, apparatuses large enough to study flames at 1g without substantial conductive loss, where maximum length scales are about $(\alpha t_{res})^{1/2}$, are insufficient for the weaker flames attainable at μg, where maximum length scales are about $(\alpha t_{rad})^{1/2}$.

Laminar Gas-Jet Flames

A fuel jet issuing into an oxidizing environment is one of the simplest types of flames. Jost [47] and Roper [48] estimated the flame height (L_f) and residence time from jet exit to flame tip (t_{jet}) by determining the height (y) where the transverse diffusion time ($d(y)^2/D$, where $d(y)$ is the stream tube width) equals the convection time ($U(y)/y$, where $U(y)$ is the axial velocity). When buoyancy and viscosity effects are negligible (momentum-controlled jets), $U(y)$ is constant and equals the jet exit velocity (U_o), whereas when buoyancy effects dominate, $U(y) \sim (gy)^{1/2}$. In either case, mass conservation requires that $d(y)^2 U(y) = d_o^2 U_o$ = constant for round jets or $d(y)U(y) = d_o U_o$ = constant for slot jets. The resulting estimated scalings for L_f and t_{jet} are given in Table 2. Transition from buoyancy-controlled to momentum-controlled conditions occurs when the time scale for the former exceeds the latter, which corresponds to $U_o > g d_o^2/D$ for either round jets or slot jets. The scalings for momentum-dominated flames presume constant U, which is reasonable for coflowing Burke-Schumann flames, but for nonbuoyant jet flames without coflow, the jet spreads and decelerates. For this situation [49]

$$L_f = \frac{U_o d_o^2}{D} \frac{1}{2Sc^{1/2}} \sqrt{\ln\left(\frac{1}{1 - c_s}\right)} \Rightarrow \qquad t_{jet} = \int_0^{L_f} \frac{dy}{U(y)} = \frac{d_o^2}{D} \ln\left(\frac{1}{1 - c_s}\right) \tag{7}$$

Because $Sc \approx 1$, the scalings of L_f and t_{jet} are similar with or without viscosity. Fig. 9 shows measurements of L_f for CH_4 flames [50]. Note that, as the scalings predict, $L_f/d_o \sim Re \equiv U_o d_o/\nu$ at both 1g and μg, and only small differences exist between 1g and μg flame lengths.

All μg studies show larger flame widths (w) at μg than 1g due to lower U and longer t_{jet} [50]. Also, w is larger at μg because the temperatures are lower (see below) and $D \sim T^{1.75}$. Because w depends on whether U is accelerating (buoyant jets), constant (nonbuoyant Burke-Schumann flames), or decelerating (nonbuoyant jets), w is more difficult to predict than is L_f [2]. The difference between 1g and μg widths decreases as Re (thus, U_o) increases (Fig. 10). The nonbuoyant widths increase slightly with Re,

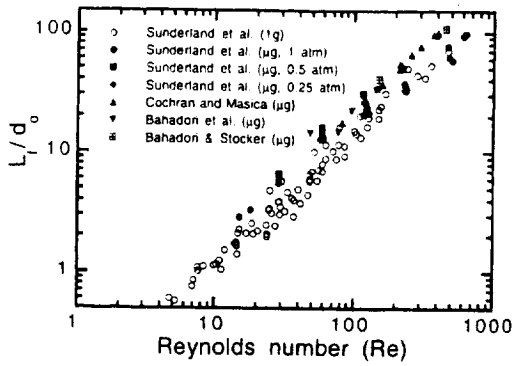

FIG. 9. Measured flame lengths, normalized by jet diameter, as a function of the jet Reynolds number for non-premixed CH_4-air jet flames at 1g and μg. Data is taken from a variety of sources and compiled in Ref. [50]. The data show a nearly linear relationship between flame length and Reynolds number, with generally longer flame lengths at μg, due to the differences between residence times under buoyancy-driven versus momentum-driven residence times.

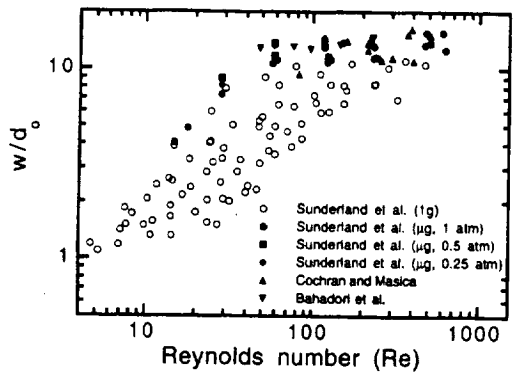

FIG. 10. Measured flame widths, normalized by jet diameter, as a function of the jet Reynolds number for non-premixed CH_4-air jet flames at 1g and μg. Data is taken from a variety of sources and compiled in Ref. [50]. The data show larger flame widths at μg due to the differences between accelerating flow at 1g versus decelerating flow at μg. The data also show that, consistent with theoretical predictions, the width is nearly independent of Reynolds number for nonbuoyant conditions, except at low *Re* where boundary-layer approximations are invalid.

whereas all aforementioned models predict self-similar flame shapes with no effect of *Re*. This may be due to axial diffusion, not considered in these models, which increases mixing over that with radial diffusion alone. This suggestion is supported by the results shown in Fig. 10 which show that w/d_o is lowest for lowest *Re* ($\approx$20), where axial diffusion is most significant, but asymptotes to fixed values at high *Re*.

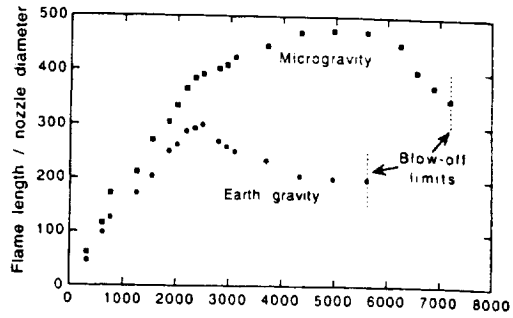

FIG. 11. Measured flame heights for non-premixed C_3H_8-air jet flames at 1g and μg [51] showing transition to turbulence. Note 1g flame lengths are shorter than μg flame lengths, even at very high Reynolds numbers.

Compared to yellow 1g flames, μg gas-jet flames are more red [49,50], indicating lower blackbody soot temperatures and presumably lower maximum flame temperatures. This occurs because t_{jet} is larger at μg and thus radiative loss effects ($\sim t_{jet}/t_{rad}$) are greater. Drop-tower [51] and space [52] experiments indicate surprisingly large and consistent radiative loss fractions (0.45–0.60) at μg compared to 0.07–0.09 at 1g, for various fuels, pressures, O_2 mole fractions, and flow rates. Thus, differences in t_{jet} at 1g and μg result in widely varying characteristics even for flames having nearly the same L_f.

Turbulent Flames

In turbulent non-premixed jet flames, D is not fixed but rather is nearly proportional to $u'L_I$. Because $u' \sim U_o$ and $L_I \sim d_o$, $L_f \sim U_o d_o^2/u'L_I \sim d_o$ for round jets; thus, L_f is independent of U_o. This prediction is supported by classical 1g experiments [53] as well as recent μg experiments [54] (Fig. 11). Note that $L_f(\mu g)/L_f(1g)$ is practically constant even beyond the transition to turbulent conditions (high U_o and *Re*). Note also that the maximum *Re* at which flame exists (the "blow-off" limit) is different at 1g and μg. This is surprising because blow-off conditions are typically controlled by behavior near the flame base [55], where buoyancy effects are often considered insignificant. This suggests that blow-off is partially affected by convection induced by the buoyant plume far above the jet exit, even at very high U_o. One would intuitively conclude that the 1g flames should blow-off at lower U_o because buoyant flow would induce higher "effective" U_o, which is consistent with Fig. 11. This shows that buoyancy effects are quite ubiquitous even under conditions commonly thought to be unaffected by buoyancy.

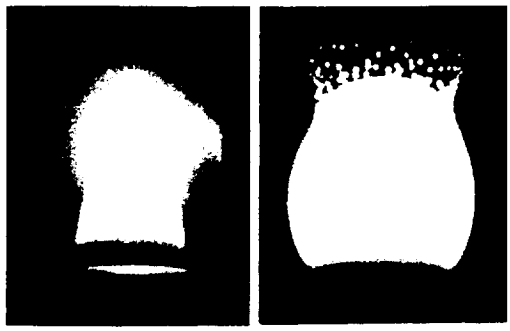

FIG. 12. Direct photographs of sooting n-C_4H_{10} nonpremixed gas-jet flames at 1g (left) and μg (right) at $Re \approx 42$, jet diameter 10 mm, showing evidence of thermophoresis-induced agglomeration at μg. Photographs courtesy of Professor O. Fujita.

Soot Formation Processes

Compared with 1g flames μg gas-jet flames have much greater tendencies to emit soot [49,56], indicating that increases in t_{jet} (thus, greater time for soot formation) plus broader regions in which composition and temperature are favorable for soot formation [56,57] outweigh lower temperatures at μg, which decreases soot formation [58]. Recent quantitative measurements [56] show peak soot-volume fractions about twice as high at μg than 1g for 50% C_2H_2/50% N_2-air flames.

Surprisingly, μg gas-jet flames exhibit "smoke points," corresponding to critical U_o below which soot is consumed within the flame, and above which soot is emitted from the flame [57]. Smoke points are expected for buoyant round-jet flames because $t_{jet} \sim U_o^{1/2}$; thus, increasing U_o increases the time available for soot formation. But for nonbuoyant flames, $t_{jet} \sim U_o^0$, suggesting no smoke point should exist. Fully elliptic numerical computations [59] show that, for some circumstances, t_{jet} does increase monotonically with U_o, which could explain smoke points for nonbuoyant flames. This behavior was suggested to result from axial diffusion effects [59], but in this case, t_{jet} should asymptote to constant values for large L_f, where axial diffusion is negligible. Thus, simple explanations of μg smoke points remain elusive. Residence-time considerations alone may be misleading; soot precursor temperature-composition-time history effects are apparently also important.

With weak convection, thermophoretic forces, which move particles toward lower temperatures, are an important effect. If convection and temperature gradients are in the same direction, the convective and thermophoretic forces may balance at some location. This leads to soot accumulation inside the flame front at μg (Fig. 12) [60], where an annulus of soot accumulation is convected by axial flow through the flame tip. Downstream, for reasons not yet explained, the soot annulus fragments, creating crown-like structures. These effects are only observable at μg where convection velocities are comparable to thermophoresis velocities, ($\approx$ 5 mm/s for the conditions of Fig. 12 [60]).

Condensed-Phase Combustion

Droplet Combustion

The first microgravity combustion experiments were isolated fuel-droplet tests conducted by Kumagai and Isoda [61]. At 1g, experimental measurements of droplet burning rates are compromised by buoyant convection, which destroys the spherical symmetry and inducing additional heat and mass transport, which alters burning rates and complicates modeling. Classical theory [62,63] predicts that burning rates for spherically symmetric buoyancy-free droplet burning are given by

$$d_{do}^2 - d_d^2 = Kt;$$

$$K \equiv (8\lambda/\rho_d C_p) \ln(1 + B) \qquad (8)$$

In experimental studies, the droplet diameter d_d could be fixed by forcing fuel through a porous sphere at rates that balances evaporation, leading to a steady mass burning rate $(\dot{m}) = (\pi/4)\rho_p d_d K$, but most experiments employ fuel droplets where d_d decreases with time. Somewhat surprisingly, many fuel-droplet results follow equation 8 well despite unsteadiness, heat losses, soot formation, and water absorption effects discussed below.

As with flame balls, steady solutions exist for spherical droplet flames even in infinite domains, with the flame front located at

$$d_f = d_d \ln(1 + B)/\ln(1 + f)$$

Whereas flame balls are convection-free, droplet flames exhibit Stefan flow due to fuel vaporization at the droplet surface. Mass conservation dictates that the Stefan velocity decays as $1/r^2$, causing temperature and concentration profiles to vary with radius in proportion to $(1 + B)^{-d_d/2r}$ rather than $1/r$ as in flame balls, although these profiles, when normalized by flame radius, are indistinguishable at large r. Unlike flame balls, heat losses are not required for stable droplet flames because the flame location cannot move away from the stoichiometric contour.

The characteristic time scale for droplet combustion is $t_{drop} \sim d_f^2/\alpha$. This leads to two extinction limits [64,65], one for small d_f where $t_{drop} < t_{chem}$ and thus fuel and oxidant cannot react before interdiffusing, and one for large d_f where $t_{drop} > t_{rad}$ and thus the temperature decrease from radiative loss

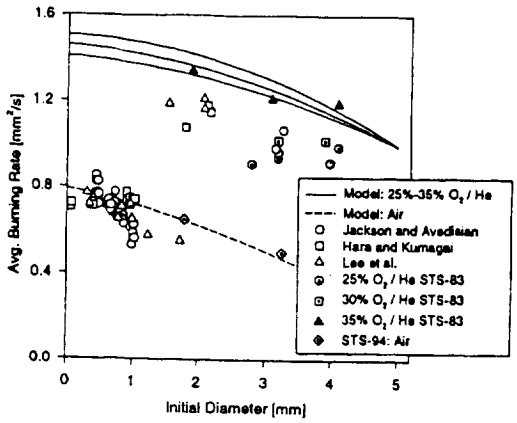

FIG. 13. Effect of initial droplet diameter (d_{do}) on quasi-steady burning rate (K) for heptane droplets burning in air and an O_2–He atmosphere at μg, showing that K decreases with increasing d_{do}, apparently because of increased accumulation of soot and gas-phase radiant species for larger d_{do} [70].

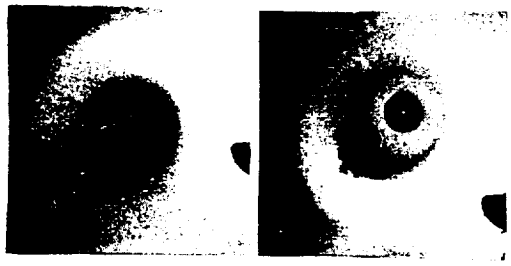

FIG. 14. Direct photographs of heptane droplets burning in air at μg showing spherically symmetric combustion (left) and a soot "tail" formed by weak convection effects (right) [68]. Photographs courtesy of Professor T. Avedisian.

reduces the reaction rate sufficiently to cause extinction. The former occurs when $d_f < (\alpha t_{chem})^{1/2}$ and the latter when $d_f > (\alpha t_{rad})^{1/2}$. Recent space experiments have reported radiative extinction of large droplets in air [66] and O_2–He [67] atmospheres. Even when radiation does not cause extinguishment, it causes a decrease in K, especially when soot formation is significant [68,69].

In experiments, K is not constant as the quasi-steady model (equation 8) predicts, but rather decreases with increasing d_{do} (Fig. 13) [70]. This suggests that nonsteady effects, specifically the diffusion of thermal energy and radiant combustion products into the far field, may be significant; this would cause changing radiative loss over time. Analogous behavior occurs in flame balls [41], where radiative loss requires ~100 s to reach steady state even in flame balls much smaller than typical droplet flames. Another indication of unsteadiness in droplet flames is that constant d_f/d_d values are not generally achieved, especially for large droplets at μg [69,70], in contrast to the predictions of the quasi-steady theory. Unsteadiness effects in droplet flames were recently analyzed by King [71]. The effect of d_{do} on K has also been proposed [68] to result from soot accumulation, which is more significant for larger d_{do} and acts to decrease net heat release and increase radiation.

As with non-premixed gas-jet flames, soot particles in μg droplet flames exhibit thermophoresis effects [72,73], leading to soot agglomeration between the droplet and flame front (Fig. 14). The agglomerates may break apart suddenly, leading to multiple burning fragments. Because velocity and temperature gradients are readily modeled in spherical droplet flames, such experimental observations enable assessment of thermophoresis effects on soot particle transport.

Another complicating factor arises in fuels that are miscible in water. The fuel may absorb water vapor from the combustion products, causing significant departure from equation 8 and reducing flammability. Such behavior is found [74,75] in methanol flames, where extinction diameters depend substantially on d_{do} due to water absorption during combustion.

Finally, in recent space experiments, flame oscillations with amplitudes comparable to the mean flame diameter have been observed [76]. The oscillation amplitude grew with time with extinction typically occurring after eight cycles. The oscillation frequency was approximately 1 Hz. Cheatham and Matalon [65] predicted oscillations of roughly the correct frequency in droplet flames of pure fuels under near-extinction conditions when the reactant Lewis numbers are sufficiently high. To date, oscillations have been reported for methanol/dodecanol (80/20 mass fraction) bicomponent droplets burning in air; it is uncertain whether oscillations also occur in pure fuels. Moreover, μg experiments in O_2–He atmospheres [67], with much higher Le, did not exhibit oscillations. One possible explanation is that droplet support fibers were used in Ref. [76] but not Ref. [67]. The fiber could increase conductive and radiative losses, which encourage oscillations [65]. Another explanation is that, because oscillations occur only near extinction conditions, depletion of oxygen (leading to extinction) was much more significant in the smaller combustion chamber used in the methanol/dodecanol experiments. Such oscillatory instabilities are discussed further in the following section.

Candle Flames

An excellent example of the differences between 1g and μg flames is seen in perhaps the most common and familiar of all combustion processes—candle flames. At 1g, candle flames are supported by air

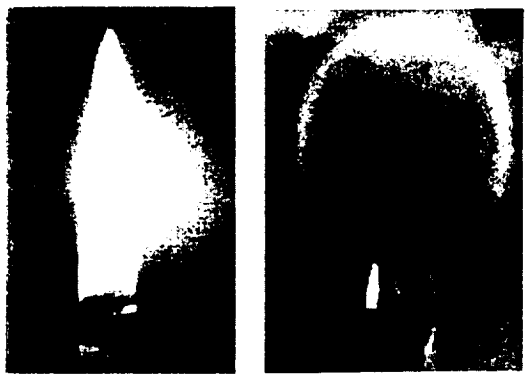

FIG. 15. Direct photographs of candle flames at 1g and μg, showing impact of buoyant flow on flame shape [77].

entrained via buoyant flow, which generates a self-sustaining flame and flow configuration. Obviously, this mechanism cannot apply at μg. The spherical diffusion equation admits steady solutions for flame balls and droplet flames without forced convection. An interesting question is whether candle flames, which are not strictly spherical, can behave similarly. Space experiments [77,78] indicate that candle flames can be steady for >45 min, with flame shapes typically hemispherical (Fig. 15). Eventually, the flames always extinguished, whereas the spherical flame model predicts that the flame would burn indefinitely. Protective screens used in the experiments may have limited the O_2 supply, eventually allowing sufficient O_2 depletion to cause extinguishment.

Before extinction, the candle-flame edge frequently advanced and retreated periodically. The oscillation amplitude increased over time, and on one retreating cycle, the entire flame extinguished. With larger wicks (thus, larger flame diameters), oscillations started spontaneously, whereas with smaller wicks, oscillations occurred only when solid objects were placed near the flame. Only a few cycles before extinction were observed in the Spacelab experiments [77], whereas hundreds of cycles were observed in the Mir experiments [78]. This is probably because the protective screen was much more permeable in the Mir experiments, thereby decreasing the O_2 depletion rate and maintaining the flame at near-extinction conditions much longer.

At least two possible explanations for these oscillations have been advanced. Cheatham and Matalon [65] showed that, near extinction, oscillatory instabilities occur in *spherically symmetric* droplet flames with radiative loss at sufficiently high Lewis numbers. Their predicted oscillation frequencies (0.7–1.4 Hz) are comparable to experimental observations, however, the differences between spherically symmetric droplet flames and roughly hemispherical candle flames were noted [65]. Alternatively, Buckmaster [79] showed that the flame "edge" separating burning and nonburning regions of non-premixed flames exhibit oscillatory behavior at (for quasi-stationary edges) $Le > 1 + 8/\beta(1 - (T_\infty/T_f)) \approx 2$ when Le for the other reactant is unity. $Le \approx 1$ for O_2 in N_2, but Le for fuel vapors is probably closer to 2; thus, edge-flame instabilities could explain the observed oscillations. While neither instability mechanism has been definitively linked to the candle-flame experiments, both predict greater propensities for oscillation with greater heat losses, which is consistent with the observation that oscillations occur near extinction.

Flame Spread over Solid Fuel Beds

Flame spread over solid fuel beds is typically classified as opposed-flow, where convection opposes flame propagation, or concurrent-flow. Because upward buoyant flow opposes flame spread, 1g downward flame spread is opposed-flow, whereas upward flame spread is concurrent-flow. At μg without forced flow, flame spread is always opposed-flow because the flame spreads toward the fresh oxidant with a self-induced velocity equal to the spread rate (S_f). At 1g, self-induced convection is negligible because buoyancy-induced flows are typically $(g\alpha_g)^{1/3} \approx 0.10$ m/s $\gg S_f$. Very few concurrent-flow flame spread have been conducted at μg [80], consequently, this section focuses on opposed-flow spread.

S_f is estimated by equating the conductive heat flux to the fuel bed ($= \lambda(\delta W)(T_f - T_v)/\delta$, where $\delta = \alpha/U$ is the thermal transport zone thickness and U is the opposed-flow velocity (forced, buoyant and/or self-induced), to rate of fuel bed enthalpy increase ($= \rho_s C_{p,s} \tau_s (T_v - T_\infty) W S_f$). Assuming mixing-limited reaction (infinite-rate chemistry), for thermally thin fuels, where heat conduction through the solid is negligible, S_f is predicted to be [81,82]

$$S_f = \frac{\pi}{4} \frac{\lambda_g}{\rho_s C_{p,s} \tau_s} \frac{T_f - T_v}{T_v - T_\infty} \tag{9}$$

Note that S_f is independent of U and P. For thermally thick fuels, where heat conduction through the solid fuel dominates, τ_s is the thermal penetration depth into the solid, estimated by equating the conductive heat flux to the fuel bed to the heat flux through the fuel ($= \lambda_{s,y}(\delta W)((T_v - T_\infty)/\tau_s)$, where the subscript y refers to the direction normal to the fuel surface). This leads to the exact solution [81]

$$\tau_s = \frac{\lambda_s(T_v - T_\infty)}{\lambda(T_f - T_v)/\delta} = \frac{\lambda_s(T_v - T_\infty)}{\lambda(T_f - T_v)} \frac{\alpha}{S_f}$$

$$\Rightarrow S_f = U \frac{\lambda \rho C_P}{\lambda_s \rho_s C_{p,s}} \left(\frac{T_f - T_v}{T_v - T_\infty} \right)^2 \tag{10}$$

Note that, unlike the thin-fuel case, for thick fuels $S_f \sim U^1 P^1$.

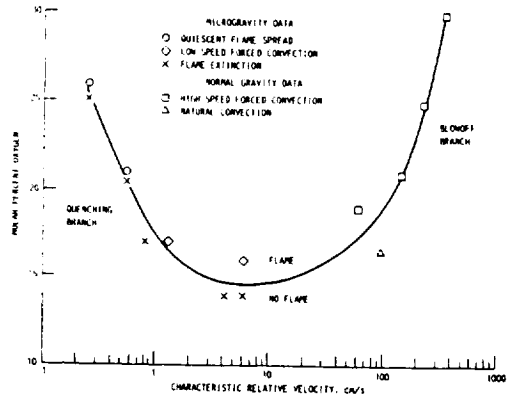

FIG. 16. Minimum mole percent O_2 in N_2 supporting flame spread over a thin solid fuel bed, as a function of the opposed flow velocity (U) [83], showing dual-limit behavior, that is, residence-time limited extinction at high U and radiative loss extinction at low U.

Dual-limit extinction behavior is observed in μg flame-spread experiments (Fig. 16) [83]. The time for thermal energy to diffuse across the convection-diffusion zone (t_{diff}) is $\delta/U = \alpha/U^2$; thus, high-U extinction occurs when $t_{diff} < t_{chem}$ or $U > (\alpha/t_{chem})^{1/2}$ and radiative extinction occurs when $t_{diff} > t_{rad}$ or $U < (\alpha/t_{rad})^{1/2}$. (Surface radiative loss may also be important, particularly at moderate and higher U [84].) Interestingly, the minimum O_2 concentration supporting combustion ($\chi_{O2,lim}$), and thus the greatest hazard, corresponds to $U \approx 0.1$ m/s, which is lower than buoyant convection at 1g, and might correspond to ventilation drafts in manned spacecraft.

A radiative loss parameter can be defined as $H \equiv t_{diff}/t_{rad} = \alpha/U^2 t_{rad}$. Because $H \sim U^{-2}$, S_f is lower at μg where U is lower and thus H is higher. Experiments [85] (Fig. 17) show that an imposed forced flow at μg increases S_f because U (sum of forced flow and S_f) increases and thus H decreases, whereas at higher U (whether buoyant or forced), S_f decreases as the high-U limit is approached. For 21% O_2 or lower, the infinite-rate chemistry prediction of equation 9, $S_f \sim U^0$, is never achieved. Only at 30% O_2 is T_f high enough that this condition is achieved.

Because $\alpha \sim P^{-1}$ and $t_{rad} \sim P^0$, $H \sim P^{-1}$, thus for thin fuels, S_f should increase with P toward the ideal (adiabatic) value (equation 9). This is confirmed by quiescent thin-fuel space experiments [86,87], which show S_f increasing from 3.2 to 5.9 mm/s as P increases from 1.0 to 2.0 atm with fixed O_2 mole fraction (0.50). For these conditions, H decreases from 24 to 3.5, thus even at the highest P, radiative effects are probably still important. This is consistent with computations [86] that predict $S_f = 12$ mm/s (almost independent of P) for adiabatic conditions for this fuel/atmosphere combination.

Neither N_2 nor O_2 emit thermal radiation; thus, for flames in O_2–N_2 atmospheres, only H_2O and CO_2 combustion products radiate significantly. For these cases, typically $a_{\bar{P}}^{-1} \approx 1.2$ m $\gg \delta$ and thus, radiative transfer is optically thin (negligible reabsorption). When $a_P\delta \geq 1$, reabsorption effects cannot be neglected. With reabsorption, some radiation is not lost and may augment conduction to increase S_f above that without radiation. This behavior is seen experimentally [88] using strongly emitting/absorbing CO_2 and SF_6 diluents (Fig. 18), where S_f is *higher* and $\chi_{O_2,lim}$ is *lower* at μg than 1g, whereas the opposite (conventional) behavior is found in nonradiant diluents (not shown). These data indicate that, for nonradiating diluents, μg is less hazardous because $\chi_{O_2,lim}$ is higher at μg than at 1g (0.21 vs. 0.16

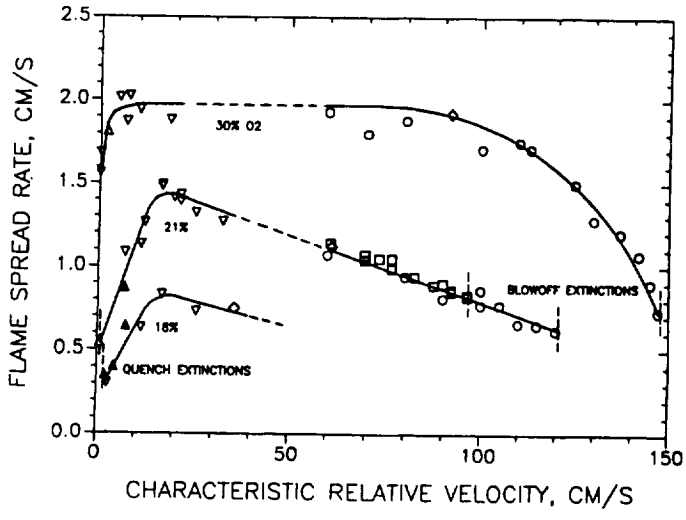

FIG. 17. Flame-spread rate over a thin solid fuel bed as a function of the opposed-flow velocity (U), for three values of the mole percent O_2 [85], showing dual-limit response. Note that the infinite-rate kinetics prediction [81,82] that the spread rate is independent of U is only satisfied at O_2 mole fractions higher than that in air.

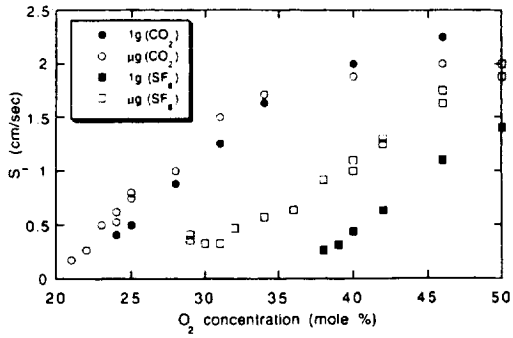

FIG. 18. Flame-spread rate over a thin solid fuel bed at 1g (downward spread) and μg as a function of O_2 mole fraction [88], showing atypical behavior in O_2–CO_2 and O_2–SF_6 atmospheres where the spread rates are higher and the minimum O_2 model fraction supporting combustion is lower at μg.

FIG. 19. Fingering patterns observed in smoldering flame spread over a thin paper fuel sample in μg [91]. Flaming combustion was inhibited by soaking the fuel sample in potassium acetate. An imposed convective velocity of 0.05 m/s flows from right to left. Grid pattern scale is 10 mm by 10 mm. Photograph courtesy of Dr. S. Olson.

for He), whereas for radiant diluents, μg is more hazardous (0.21 vs. 0.24 for CO_2). This is particularly significant considering that CO_2-based fire suppression systems will be used on the International Space Station. To date, flame spread calculations have employed optically thin radiation models with constant a_P [86,87] or variable depending on local temperature and composition [80] and thus cannot assess reabsorption effects.

These discussions pertain to thin fuels, for which steady μg spread is possible because theoretically $S_f \sim U^0$. For thick fuels, $S_f \sim U^1$, thus S_f is indeterminate for quiescent μg conditions ($U = S_f$). When unsteady solid-phase conduction is considered, $\tau_s \sim (\alpha_s t)^{1/2}$, which results in $S_f \sim t^{-1/2}$ [89]. Consequently, all fuel beds at quiescent μg conditions eventually become thermally thin (penetration depth greater than the bed thickness) unless the radiative effects, discussed later, are considered. Of course, flames may extinguish due to large δ (thus large radiative loss) before reaching steady-state, thermally thin conditions.

A difficulty in comparing space experiments to two-dimensional model predictions is that the fuel bed width W (30 mm for thin fuels [86,87] and 6.2 mm for thick fuels [89]) is smaller than the *thermal* transport zone thickness (δ). Consequently, these experiments can hardly be considered two-dimensional. Both lateral heat loss, which retards spread, and lateral O_2 influx, which enhances spread, are probably important, thus their effects may partially cancel. Some authors [86] suggest that radiative losses decrease δ to values much smaller than $\alpha/U = \alpha/S_f$, but the *oxygen* transport zone thickness (δ_{O_2}) is still D_{O_2}/U, because no analog to radiative loss exists for O_2 transport. Because $Le = \alpha/D_{O_2} \approx 1$, δ_{O_2} is nearly the same as δ in adiabatic flames. Thus, the μg flames mentioned above have probably benefited substantially from lateral O_2 influx, especially for lower pressures and O_2 mole fractions, where $\delta/W \sim \alpha/S_f W$ is largest. In fact, S_f might be *higher* at smaller W due to lateral O_2 influx. Space experiments using cylindrical fuel rods are planned [90] to examine truly two-dimensional spread.

Recently, a surprising observation of fingering fronts was found in space experiments using paper samples treated to inhibit flaming combustion but allow smoldering propagation (Fig. 19) [91]. Fingering was observed at μg when $U < 50$ mm/s, whereas smooth fronts were observed at 1g for all U. This was proposed [91] to result from limited O_2 mass transport at μg with low U, which caused the O_2 consumption regions to become localized spots instead of continuous fronts. This proposition does not explain why heat conduction does not smooth out potential fingers as it does (for example) in premixed-gas flames with $Le > 1$. The following alternative explanation is proposed here. Gas-phase heat transport occurs on the length scale $\delta \sim \alpha/U$, and solid-phase transport occurs on the scale $\delta_s \sim \alpha_s/u_s$ where u_s is the smolder front velocity and α_s the solid thermal diffusivity. Oxygen transport occurs only through the gas phase on the scale $D_{O_2}/U \approx \alpha/U \sim \delta$. Radiative loss can suppress heat transport through the gas, but no corresponding effect on O_2 transport can occur. Thus, at low U, the effective Le is $\alpha_s/D_{O_2} \ll 1$. At higher U or at 1g, δ is smaller, gas-phase heat transport dominates, and radiative effects are weaker; thus, the effective Le is $\alpha/D_{O_2} \approx 1$. These assertions are consistent with estimates [91]

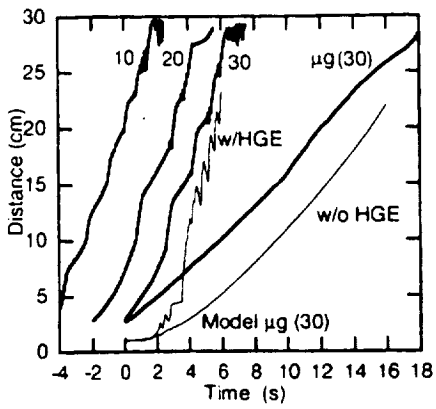

FIG. 20. Measured (thick lines) and computed (thin lines) flame position versus time for flame spread over a 1-butanol pool 20-mm wide and 25-mm deep [97]. The 10, 20, and 30 notations refer to the opposed-flow velocities (U) in cm/s. Both computed results are for μg conditions, U = 30 cm/s, either with or without hot gas expansion (HGE). The comparison of predicted and measured results suggests a very strong influence of expansion, which is much less effective in the experiment because of the relaxation of expansion in the transverse dimension, a factor not captured within the two-dimensional model.

of the relative importance of gas-phase and solid-phase transport. Both premixed [27,39] and non-premixed [92,93] flames with effective $Le < 1$ exhibit diffusive-thermal instabilities that cause fingering patterns, whereas for Le $\geq$ 1, the fronts are stable. This explanation is also consistent with 1g experiments [94] on horizontal fuel beds burning in oxidant channels of adjustable vertical height. At small heights or low U, fingering similar to Fig. 19 was observed. In this case, conductive loss to the channel ceiling causes suppression of gas-phase heat transfer. Apparently, in both cases, the key factor is suppression of gas-phase heat transfer while allowing solid-phase heat transfer, which reduces the effective Le (though this factor was not mentioned in Ref. [91] or Ref. [94].)

Flame Spread over Liquid Fuel Pools

Flame spread over liquid fuels encompasses practically all solid-fuel flame spread phenomena discussed above, plus liquid-phase flow effects. Typically, $T_v - T_\infty$ is smaller for liquid than solid fuels, thus S_f is higher. Also, if $T_v - T_\infty$ is small, some fuel prevaporization occurs even at $T = T_\infty$, thus partially premixed gas-phase combustion phenomena may occur. Because of the fuel surface temperature gradient upstream of the flame, surface tension gradients are produced that cause the surface layer to move upstream (away from the flame), which increases S_f. At 1g, this heated liquid layer must lie near the surface, whereas at μg, no limitation exists.

Experiments at 1g, summarized in [95], show that at low fuel temperatures, the average S_f is small (typically 10 mm/s) and the spread alternates between a fast "jump" velocity and a slow "crawl" velocity. At higher fuel temperatures, S_f is faster and steady. For the conditions exhibiting pulsating spread at 1g, μg flame spread cannot be maintained, whereas for the conditions exhibiting uniform spread at 1g, steady spread is also exhibited at μg [96]. Pulsating spread has never been observed at μg. No definitive explanation for these observations has been advanced. For the conditions exhibiting pulsating spread at 1g and no spread at μg, flame spread is still different at 1g and μg when forced flows comparable to buoyancy-induced convection (U = 0.30 m/s) are imposed (Fig. 20) [97]. Specifically, 1g spread is almost unaffected by the imposed flow, but μg spread is *steady* with S_f being lower ($\approx$15 mm/s) than either the 1g jump velocity ($\approx$100 mm/s) or crawl velocity ($\approx$22 mm/s).

Detailed numerical modeling [98] predicts pulsating spread at μg for the conditions of Fig. 20 and values of S_f much closer to the measured 1g S_f. Remarkably, if thermal expansion is artificially suppressed, good agreement between the model and μg experiments is found. It is proposed [97] that this agreement results from three-dimensional effects; specifically, in the experiment, flow induced by thermal expansion is relaxed in the lateral dimension, whereas the two-dimensional model does not permit this. That three-dimensional effects might dominate is surprising considering that, for this flame, $\delta/W \sim \alpha/UW \approx 0.02$, thus, $\delta \ll W$. Also, this hypothesis does not explain why pulsating flame spread is observed at 1g but not μg. Consequently, in the case of liquid-fuel flame spread, μg experiments have identified limitations in our current understanding of combustion processes at 1g.

Recommendations for Future Studies

Reabsorption Effects

The μg studies described here suggest new unresolved issues and opportunities for further improvements in understanding. Perhaps the most important are the effects of reabsorption of emitted radiation, including both reabsorption by the emitting gas and, in two-phase combustion, absorption by the condensed phase. All radiative effects discussed above are critically dependent on the degree of reabsorption. To study reabsorption effects requires radiatively active diluents (CO_2, SF_6), high pressures and/or large systems. All of these conditions lead to higher Gr_d at 1g and thus turbulent flow. Hence, μg

experiments enable study of reabsorption effects without the additional complications due to turbulence.

Reabsorption effects are important not only to μg studies but also to combustion at high pressures and in large combustors. For example, at 40 atm, typical of premixed-charge internal combustion engines, $a_P \approx 18\ m^{-1}$, thus, $a_P^{-1} = 0.045$ m, for stoichiometric combustion products. Because this length scale is comparable to cylinder radii, reabsorption effects within the gas cannot readily be neglected. Simple estimates [99] indicate radiative loss may influence flame quenching by turbulence in lean mixtures. Similarly, reabsorption cannot be neglected in atmospheric-pressure furnaces larger than $a_P^{-1} \approx 2.2$ m. Moreover, many combustion devices employ exhaust-gas or flue-gas recirculation; for such devices, the unburned mixtures contain significant amounts of absorbing CO_2 and H_2O.

Although reabsorption of emitted radiation could affect practically all types of flames reviewed here, to date, reabsorption effects have been studied only for propagating premixed-gas flames [24,26], flame balls [45], and flame spread over thermally thin fuels [88]. All have shown substantial differences from optically thin behavior. Two examples of effects expected for other flames are given below.

Reabsorption effects could be substantially more important for droplet combustion than for flame spread over solid fuels because for droplets, the Stefan flow severely limits heat conduction to the droplet surface. This is why heat release (B) affects burning rates (K) only weakly (logarithmically) (equation 8). Radiative transfer is unaffected by the Stefan flow. Equation 8 is readily extended to include surface radiative flux (q_r):

$$\Omega = \ln\left(1 + \frac{B}{1 - R/\Omega}\right);\ R \equiv \frac{q_r d_d C_P}{2\lambda L_v};\ \Omega \equiv \frac{K\rho_d C_P}{8\lambda} \tag{11}$$

Figure 21 shows the predictions of equation 11. (Although equation 11 has apparently not been presented previously, numerical studies [100,101] have shown qualitatively similar predictions. Moreover, these studies show that typical radiative absorption lengths for liquid fuels at relevant wavelengths are on the order of 1 mm, thus large droplets could absorb most incident radiation.) For spherical shells of radiant combustion products having thickness $\delta \ll d_f$, $q_r \approx A\delta/4$, then for typical values $B = 8.5$, $A = 2 \times 10^6\ W/m^3$, $\delta = 10$ mm, $d_d = 5$ mm, $C_p = 1400$ J/kgK, $\lambda = 0.07$ W/mK, and $L_v = 400$ kJ/kg, equation 11 predicts $R = 0.63$ and $\Omega/\Omega_{R=0} = 1.11$; thus, moderate effects of radiative transfer are expected. For droplets in radiatively active diluents such as CO_2, the effect could be much stronger. Using the P1 approximation, for a sphere of unit emissivity in an infinite gray gas, $q_r = [4/(2 + 3 a_P d_d/2)]\sigma(T^4 - T_\infty^4)$ [102]. Using volume-averaged properties $T = 1000$ K and $a_{P(CO_2)} = 20\ m^{-1}$, $R = 18$ and thus $\Omega/\Omega_{R=0} = 8.0$, indicating radiation dominates heat transport. As discussed later, at high pressures radiative effects may prevail even in O_2–N_2 atmospheres.

Flame spread over thermally thick fuel beds in quiescent atmospheres at μg is typically considered inherently unsteady [89], however radiative transfer to the fuel bed could enable steady spread. If the flame is modeled by an isothermal volume with dimensions $\delta \times \delta \times W$, radiation induces a radiative flux $A\delta^2 W = A(\alpha^2/S_f^2)W$ that augments the conductive flux $\lambda(\delta W)(T_f - T_\infty)/\delta$. Equating this total heat transfer to $\rho_\infty C_{P,\infty} \tau_\infty (T_\infty - T_\infty) WS_f$ yields

$$S_f = \left[\frac{A\alpha_g^2}{\sqrt{\alpha_g \rho_\infty C_{P,\infty} \lambda_\infty (T_\infty - T_\infty)} - \lambda_g (T_f - T_\infty)}\right]^{1/2} \tag{12}$$

which vanishes without gas radiation ($A = 0$). Thick-fuel space experiments in O_2–CO_2 or O_2–SF_6 atmospheres could be employed to check for steady spread and test the accuracy of equation 12.

Whereas optically thin radiation modeling is reasonably straightforward, modeling of spectrally dependent emission and absorption is challenging because local fluxes depend on the entire radiation field, not just local scalar properties and gradients. Some relevant computations have employed gray-gas models [74], but recent studies [26,103] show that these methods are probably inaccurate because of the wide variation in spectral absorption coefficient with temperature, species, and wavelength. Comparisons of various radiative treatments for small one-dimensional non-premixed flames have been made [103]. Comparisons for larger, multidimensional systems would be valuable. Moreover, recent studies of μg soot formation [52,56,57] may enable improved modeling of soot radiation at μg.

High-Pressure Combustion

All practical combustion engines operate at pressures much higher than atmospheric. The impact of buoyancy for premixed flames scales as $t_{chem}/t_{vis} \sim (g\alpha/S_L^2)^{2/3} \sim P^{n-4/3}$, where n is the overall reaction order ($S_L \sim P^{n/2-1}$). Because, typically, $n < 4/3$ for weak mixtures [104], where buoyancy effects are most important, the impact of buoyancy increases with pressure. Also, as discussed earlier, radiation effects are more difficult to assess at higher pressure due to increased interference from buoyant transport. Nevertheless, few high-pressure μg combustion experiments have been performed. High-pressure droplet combustion experiments [105] revealed substantial but different increases in K with P at 1g and μg. Radiative effects were not discussed but could have been important, because in equation 11,

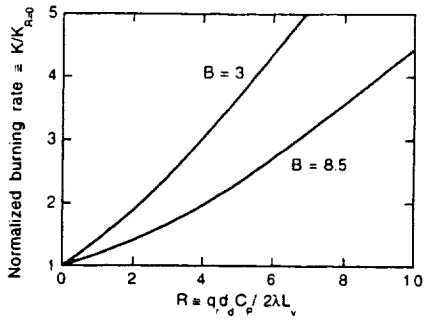

FIG. 21. Predicted effect of radiative heat transport coefficient (R) on droplet burning rate constant referenced to the value without radiative transport, showing importance of absorption of radiation at the droplet surface on the resulting burning rate. $B = 3$ and $B = 8.5$ are characteristic of methanol and heptane, respectively, burning in air.

the only pressure-dependent factor is $q_r \sim \Lambda \sim P^1$, thus in Fig. 21, $R \sim P$. (For most flames, length scales decrease with increasing P, which would decrease radiative effects; but for droplet flames, d_f depends only on stoichiometry [75,76].) Consequently, further assessment of radiative effects in high-pressure droplet combustion and other types of flames appears warranted.

Three-Dimensional Effects

In earlier sections, effects of lateral heat and mass transport on flame spread were discussed. To assess three-dimensional effects, μg experiments with varying fuel bed width (W) are needed. Complementary three-dimensional modeling using codes such as those developed by NIST [106], extended to include gas-phase radiation, would be instructive. An approximate but much less expensive approach would be to incorporate volumetric terms $6\lambda(T(x, y) - T_\infty)/W^2$ and $6\rho D_i(Y_i(x, y) - Y_{i,\infty})/W^2$, where x and y are the coordinates parallel and perpendicular to the fuel bed, into the two-dimensional model to account for lateral heat losses and lateral diffusion of each species i.

Another three-dimensional effect is found in the development of flame balls from ignition kernels. Currently, it is known that large flame balls are linearly unstable to three-dimensional disturbances for weak loss (Fig. 5), but the transition from splitting flame balls to stable flames is not well understood, nor can the number of flame balls produced from an ignition source be predicted. Modeling using three-dimensional premixed flame codes [107] is needed.

Gas-Jet Flames

Table 2 shows predicted scalings of flame lengths (L_f) and residence times (t_{jet}) for buoyant and nonbuoyant round-jet and slot-jet flames. Despite numerous investigations of round-jet flames at μg, no μg slot-jet results are available to test those predictions. Currently, it is unknown whether slot-jet flames at μg would exhibit smoke points or whether this information could be used to explain smoke points in μg round-jet flames. Because L_f depends on g for buoyant slot-jet but not round-jet flames, L_f should be quite different at 1g and μg for slot-jets but not round-jets. Residual accelerations in aircraft μg experiments will be more problematic for slot-jet than round-jet flames because $t_{jet} \sim g^{-1/2}$ for buoyant round-jet flames whereas $t_{jet} \sim g^{-1/3}$ for slot-jet flames.

There has been little investigation of blow-off behavior of laminar gas-jet flames at μg. Dual-limit behavior might occur for flames of fixed-mass flow rate but varying d_o, with short residence time extinction at small d_o ($t_{jet} \sim d_o^2/U_o$) and radiative extinction at large d_o (thus, large t_{jet}). Experiments should be conducted by diluting the fuel rather than increasing U_o to obtain blow-off without transition to turbulence. In this way, dual-limit behavior has been observed at 1g [92] with short residence time and conductive loss (to the burner rim) extinction branches.

Quasi-Steady Spherical Diffusion Flames

As discussed previously, comparing predicted radiative extinction limits of droplet flames to experiments is problematic because quasi-steady conditions may not be obtained, because extinction occurs for sufficiently large droplet and flame diameters, but the droplet diameter decreases throughout its life. Numerical models can account for transient effects, but the multidimensional ignition process is difficult to model quantitatively. Comparisons of droplet experiments and computations to corresponding results obtained using fuel-wetted porous spheres would be most interesting. The fuel should be forced through the porous sphere at slowly increasing rates until extinction occurs when $d_f > (\alpha t_{rad})^{1/2}$, thus obtaining truly quasi-steady extinction. Long μg durations would be required to establish steady diffusion-dominated far-field temperature and composition profiles (thus, steady radiative loss). Some preliminary results have been obtained in aircraft experiments [108] but were severely compromised by the residual g levels. Candle flames are similar to wetted porous spheres, though without true spherical symmetry or any means to control or measure the instantaneous d_d.

A simpler related experiment employs porous spheres through which gaseous fuel is forced at prescribed $\dot{m}$, resulting in a flame diameter $d_f \approx \dot{m}C_p/2\pi\lambda\ln(1 + f)$. Some drop-tower experiments using this configuration have been reported [109,110], although steady-state conditions were not obtained due to short μg durations. Steady-state behavior appears unlikely given the $\dot{m}$ (thus, air consumption rates) and chamber sizes employed to date; near-wall

oxygen depletion would be significant over the times required to reach steady-state ($\geq$10 s [110]). Steady-state behavior might be obtained in drop-towers by using smaller $\dot{m}$ and diluted fuel with enriched oxygen atmospheres to increase f and thus decrease d_f and $t_{drop} \sim d_f^2/\alpha$.

Catalytic Combustion

Catalytic combustion holds promise for reduced emissions and improved fuel efficiency in many combustion systems [111,112]. Because catalysis occurs at surfaces, it is inherently multidimensional and/or unsteady, requiring reactant transport to the surface and heat and products transport from the surface. Although boundary-layer approximations can be invoked, probably the only truly one-dimensional steady catalytic configuration is a spherical surface immersed in nonbuoyant quiescent premixed gas—a "catalytic flame ball." In this case, r_f is fixed but the surface temperature T_s and fuel concentration Y_s are unknown. These are related through the energy conservation (including surface radiation) and diffusion equations to obtain the surface reaction rate in moles per second (Θ):

$$\Theta(Y_s, T_s) = \rho_s D_s r_s Y_\infty (1 - Y_s/Y_\infty)/M$$

$$\frac{Y_s}{Y_\infty} = 1 - Le\left(\frac{T_s - T_\infty}{T_{ad} - T_\infty}\right)\left(1 + \frac{\sigma \varepsilon_s r_s (T_s^4 - T_\infty^4)}{\lambda_s (T_s - T_\infty)}\right) \quad (13)$$

where ε_s is the surface emissivity and properties with the subscript s are evaluated at $T = T_s$. By varying r_s, Y_∞, pressure, and diluent gas, $\Theta(T, Y)$ can be inferred from equation 13 and the *measured* T_s. Of course, conditions must be unfavorable for initiation of propagating flames or flame balls that stand off from the surface.

Chemical Models

An important contribution of μg combustion experiments has been improved understanding of extinction processes, which are inherently related to finite-rate chemistry. To obtain closure between experiments and computations, accurate chemical models are needed. For lean premixed hydrocarbon-air flames, most models [21,26] predict higher S_L and leaner flammability limits than experimental observations [22,33,113]. The discrepancy seems larger than experimental uncertainty or unaccounted heat losses could explain. In contrast, for H_2-air flame balls [45] and 1g strained premixed H_2-air flames [114], these chemical models predict smaller balls, lower S_L, and richer flammability limits than experiments. These chemical models predict S_L in mixtures away from extinction limits very faithfully. The discrepancies result largely from differences in rates for H + O_2 + M reactions, particularly the Chaperon efficiencies of various M species [45]. These reactions are extremely important in near-limit flames due to competition between chain-branching and chain-inhibiting steps near limits [21] but are much less important away from limits. Further scrutiny of the rates for these reactions at intermediate temperatures (1100–1400 K) would be welcomed.

Conclusions

Our understanding of combustion fundamentals has been broadened by μg experiments into regimes not previously explored. In particular, these experiments have helped integrate radiation into flame theory. Although flame radiation has long been recognized as an important heat-transfer mechanism in large fires [115], its treatment has largely been ad hoc because of the difficulty of predicting soot formation. Also, large-scale fires at 1g are inevitably turbulent, leading to complicated flame-flow interactions. Small-scale μg flames are laminar, often soot-free, and have significant influences of radiation. As a result of radiation effects, both premixed and non-premixed flames have exhibited dual-limit extinction behavior, with residence time-limited extinction at high strain, or curvature and radiative loss-induced extinction at low strain or curvature. The high-strain limit is readily observed at 1g; when forced flow is absent, buoyant flow causes this strain. For weak mixtures, these limits converge, but the convergence and the entire low-strain extinction branch can only be seen at μg. This dual-limit behavior is observed for stretched and curved premixed-gas flames, strained non-premixed flames, isolated fuel droplets, and flame spread over solid fuels. Besides radiative effects, μg studies have enabled observation and clarification of numerous other phenomena, for example, thermophoresis effects in soot formation, spherically symmetric droplet burning, diffusion-controlled premixed flames (flame balls), and flame instabilities in droplets and candle flames. Considering the rapid progress made recently, further advances are certain to occur. It is hoped that this report on the current state of understanding will help motivate and inspire such advances.

Nomenclature

a_P	Planck mean absorption coefficient
A	flame surface area
B	transfer number (chemical enthalpy generation/enthalpy needed for fuel evaporation)
c_s	stoichiometric molar ratio of fuel to air
C_P	constant-pressure heat capacity

d	characteristic flow-length scale or tube diameter
d_f	droplet flame diameter
d_d	droplet diameter
d_{do}	droplet initial diameter
d_o	jet exit diameter (round jets) or slot width (slot jets)
D	mass diffusivity
E	overall activation energy of the heat-release reactions
f	stoichiometric fuel to air mass ratio
g	acceleration of gravity
g_o	earth gravity
Gr_d	Grashof number based on characteristic length scale (d) = gd^3/ν^2
h	heat transfer coefficient in a cylindrical tube = $16\lambda/d^2$
H	radiative loss parameter for flame spread = $t_{diff}/t_{rad} = \alpha/U^2 t_{rad}$
K	droplet burning rate constant (equation 8)
L_f	flame length for gas-jet flame
L_I	turbulence integral scale
L_v	latent heat of vaporization of liquid fuel
Le	Lewis number (α/D = thermal diffusivity/reactant mass diffusivity)
$\dot{m}$	mass burning rate
M	fuel molecular weight
P	pressure
r	radial coordinate
r_f	flame radius
R	scaled flame radius (eq 6); radiation parameter (eq 11)
R_g	gas constant
Re	jet Reynolds number = $U_o d_o/\nu$
S_f	flame spread rate over solid fuel bed
S_L	premixed laminar burning velocity
$S_{L,lim}$	burning velocity at the flammability limit
Sc	Schmidt number = ν/D
t_{chem}	chemical time scale
t_{diff}	thermal diffusion time scale = α/U^2
t_{drop}	droplet flame time scale = d_f^2/α
t_{inv}	inviscid buoyant transport time scale
t_{jet}	residence time of non-premixed jet flame
t_{rad}	radiative loss time scale
t_{vis}	viscous buoyant transport time scale
T	temperature
T_{ad}	adiabatic flame temperature
u'	turbulence intensity
U	convection velocity
U_y	local axial velocity in counterflow configuration
U_o	jet exit velocity
w	gas-jet flame width
W	solid fuel bed width
y	axial coordinate
Y	fuel mass faction
α	thermal diffusivity
β	nondimensional activation energy = $E/R_g T_f$
$\chi_{O_2,lim}$	minimum oxygen concentration supporting combustion
δ	flame thickness
γ	gas specific heat ratio
λ	thermal conductivity
Λ	radiative heat loss per unit volume = $4\sigma a_p(T_f^4 - T_\infty^4)$
ν	kinematic viscosity
ρ	density
τ_s	fuel bed half-thickness (thin fuel) or thermal penetration depth (thick fuel)
σ	Stefan–Boltzmann constant
Σ	flame stretch rate

Subscripts

d	droplet surface condition
f	flame front condition
s	solid-fuel or solid-surface condition
v	solid- or liquid-fuel vaporization condition
∞	ambient conditions

Acknowledgments

The author expresses his deepest gratitude to the NASA-Lewis Research Center for supporting his μg combustion work for more than 10 years. Comments from Tom Avedisian, Yousef Bahadori, John Buckmaster, Mun Choi, Dan Dietrich, Fred Dryer, Gerard Faeth, Guy Joulin, Yiguang Ju, Kaoru Maruta, Vedha Nayagam, Takashi Niioka, Sandra Olson, Howard Ross, Kurt Sacksteder, Dennis Stocker, Peter Sunderland, Gregory Sivashinsky, James Tien, Karen Weiland, Forman Williams, and anonymous reviewers have been invaluable in preparing this paper. The author also thanks numerous others who offered useful suggestions that could not be accommodated because of space limitations.

REFERENCES

1. Sacksteder, K. R., in *Twenty-Third Symposium (International) on Combustion*, The Combustion Institute, Pittsburgh, 1990, pp. 1589–1597.
2. Law, C. K. and Faeth, G. M., *Prog. Energy Combust. Sci.* 20:65–113 (1994).
3. *Microgravity Combustion Science: 1995 Program Update*, NASA TM-106858, 1995.
4. Kono, M., et al., in *Twenty-Sixth Symposium (International) on Combustion*, The Combustion Institute, Pittsburgh, 1996, pp. 1189–1199.
5. Coward, H. and Jones, C., *U.S. Bureau of Mines Bulletin* 503 (1952).
6. Giovangigli, V. and Smooke, M., *Combust. Sci. Technol.* 87:241–256 (1992).
7. Levy, A., *Proc. R. Soc. London* A283:134–145 (1965).
8. Wang, Q. and Ronney, P. D., "Mechanisms of Flame Propagation Limits in Vertical Tubes," Spring Technical Meeting, Eastern/Central States Section of the

The Combustion Institute, New Orleans, LA, March 15–17, 1993 Paper No. 45.
9. Buckmaster, J. D. and Mikolaitis, D., *Combust. Flame* 45:109–119 (1982).
10. Krivulin, V. N., Kudryavtsev, E. A., Baratov, A. N., Badalyan, A. M., and Babkin, V. S., *Combust. Expl. Shock Waves* 17:37–41 (1981).
11. Jarosinsky, J., Strehlow, R. A., and Azarbarzin, A., in *Nineteenth Symposium (International) on Combustion*, The Combustion Institute, Pittsburgh, 1982, pp. 1549–1557.
12. Patnaik, G. and Kailasanath, K., in *Twenty-Fourth Symposium (International) on Combustion*, The Combustion Institute, Pittsburgh, 1992, pp. 189–195.
13. Spalding, D. B., *Proc. R. Soc. London* A240:83–100 (1957).
14. Buckmaster, J. D., *Combust. Flame* 26:151–162 (1976).
15. Joulin, G. and Clavin, P., *Acta Astronautica* 3:223–240 (1976).
16. Jarosinsky, J., *Combust. Flame* 50:167–175 (1983).
17. Aly, S. L. and Hermance, C. E., *Combust. Flame* 40:173–185 (1981).
18. Williams, F. A., *Combustion Theory*, 2nd ed., Benjamin-Cumming, Menlo Park, 1985.
19. Abbud-Madrid, A. and Ronney, P. D., in *Twenty-Third Symposium (International) on Combustion*, The Combustion Institute, Pittsburgh, 1990, pp. 423–431.
20. Lakshmisha, K. N., Paul, P. J., and Mukunda, H. S., in *Twenty-Third Symposium (International) on Combustion*, The Combustion Institute, Pittsburgh, 1990, pp. 433–440.
21. Law, C. K. and Egolfopoulos, F. N., in *Twenty-Fourth Symposium (International) on Combustion*, The Combustion Institute, Pittsburgh, 1992, pp. 137–144.
22. Ronney, P. D., in *Twenty-Second Symposium (International) on Combustion*, The Combustion Institute, Pittsburgh, 1988, pp. 1615–1623.
23. Strehlow, R. A. and Reuss, D. L., in *Combustion Experiments in a Zero Gravity Laboratory* (T. H. Cochran, ed.), Progress in Aeronautics and Astronautics, vol. 73, AIAA, New York, 1981, pp. 61–89.
24. Abbud-Madrid, A. and Ronney, P. D., *AIAA J.* 31:2179–2181 (1993).
25. Joulin, G. and Eudier, M., in *Twenty-Second Symposium (International) on Combustion*, The Combustion Institute, Pittsburgh, 1988, pp. 1579–1585.
26. Ju, Y., Masuya, G., and Ronney, P. D., in *Twenty-Seventh Symposium (International) on Combustion*, The Combustion Institute, Pittsburgh, 1998, pp. 2619–2625.
27. Clavin, P. *Prog. Energy Combust. Sci.* 11:1–59 (1985).
28. Ronney, P. D. and Sivashinsky, G. I., *SIAM J. Appl. Math.* 49:1029–1046 (1989).
29. Ronney, P. D., *Combust. Sci. Technol.* 59:123–141 (1988).
30. Farmer, J. R. and Ronney, P. D., *Combust. Sci. Technol.* 73:555–574 (1990).
31. Lewis, B. and von Elbe, G., *Combustion, Flames, and Explosions of Gases*, 3rd ed., Academic Press, Orlando, FL, 1987.
32. Buckmaster, J. D. and Mikolaitis, D., *Combust. Flame* 47:191–204 (1982).
33. Guo, H., Ju, Y., Maruta, K., Niioka, T., and Liu, F., *Combust. Flame* 109:639–646 (1997).
34. Ju, Y., Guo, H., Liu, F., and Maruta, K., *Fluid Mech*, in press.
35. Buckmaster, J. D., *Combust. Theory Modeling* 1:1–11 (1997).
36. Zeldovich, Ya. B., *Theory of Combustion and Detonation of Gases*, Academy of Sciences (USSR), Moscow, 1944.
37. Deshaies, B. and Joulin, G., *Combust. Sci. Technol.* 37:99–116 (1984).
38. Buckmaster, J. D. and Weeratunga, S., *Combust. Sci. Technol.* 35:287–296 (1984).
39. Ronney, P. D., *Combust. Flame* 82:1–14 (1990).
40. Ronney, P. D., Whaling, K. N., Abbud-Madrid, A., Gatto, J. L., and Pisowicz, V. L., *AIAA J.* 32:569–577 (1994).
41. Ronney, P. D., Wu, M. S., Weiland, K. J., and Pearlman, H. G., *AIAA J.* 36:1361–1368 (1998).
42. Buckmaster, J. D., Joulin, G., and Ronney, P. D., *Combust. Flame* 79:381–392 (1990).
43. Lee, C. and Buckmaster, J. D., *SIAM J. Appl. Math.* 51:1315–1326 (1991).
44. Buckmaster, J. D., Smooke, M., and Giovangigli, V., *Combust. Flame* 94:113–124 (1993).
45. Wu, M. S., Liu, J. B., and Ronney, P. D., in *Twenty-Seventh Symposium (International) on Combustion*, The Combustion Institute, Pittsburgh, 1998, pp. 2543–2550.
46. Maruta, K., Yoshida, M., Guo, H., Ju, Y., and Niioka, T., *Combust. Flame* 112:181–187 (1998).
47. Jost, W., *Explosions and Combustion Processes in Gases*, McGraw-Hill, New York, 1946.
48. Roper, F., *Combust. Flame* 29:219–226 (1977).
49. Haggard, J. B. and Cochran, T. H., *Combust. Sci. Technol.* 5:291–298 (1972).
50. Sunderland, P. B., Mendelson, B. J., Yuan, Z. G., and Urban, D. L., *Combust. Flame* 116:376–386 (1999).
51. Bahadori, M. Y., Stocker, D. P., Vaughan, D. F., Zhou, L. and Edelman, R. B., in *Modern Developments in Energy Combustion and Spectroscopy* (F. A. Williams, A. K. Oppenheim, D. B. Olfe, and M. Lapp, eds.), Pergamon Press, 1993, pp. 49–66.
52. Urban, D. L., Yuan, Z. G., Sunderland, P. B., Voss, J. E., Lin, K. C., Dai, Z., Sun, K., and Faeth, G. M., *AIAA J.* 36:1346–1360 (1998).
53. Hottel, H. C. and Hawthorne, W. R., in *Third Symposium (International) on Combustion*, The Combustion Institute, Pittsburgh, Williams & Wilkins, Baltimore, 1949, pp. 254–266.
54. Hedge, U., Yuan, Z. G., Stocker, D., and Bahadori, M. Y., in *Proceedings of the Fourth International Microgravity Combustion Workshop*, NASA Conference Publication 10194, 1997, pp. 185–190.

55. Pitts, W. M., in *Twenty-Second Symposium (International) on Combustion*, The Combustion Institute, Pittsburgh, 1988, pp. 809–816.
56. Greenberg, P. S. and Ku, J. C., *Combust. Flame* 108:227–230 (1997).
57. Sunderland, P. B., Mortazavi, S., Faeth, G. M., and Urban, D. L., *Combust. Flame* 96:97–103 (1994).
58. Glassman, I., in *Twenty-Second Symposium (International) on Combustion*, The Combustion Institute, Pittsburgh, 1988, pp. 295–311.
59. Mortazavi, S., Sunderland, P. B., Jurng, J., Köylü, Ü. Ö., and Faeth, G. M., *AIAA paper* 93-078 1993.
60. Fujita, O., Ito, K., Ito, H., and Takeshita, Y., in *Proceedings of the Fourth International Microgravity Combustion Workshop*, NASA Conference Publication 10194, 1997, pp. 217–222.
61. Kumagai, S. and Isoda, H., in *Sixth Symposium (International) on Combustion*, The Combustion Institute, Pittsburgh, 1957, pp. 726–731.
62. Spalding, D. B., in *Fourth Symposium (International) on Combustion*, Williams & Wilkins, Baltimore, 1953, pp. 847–864.
63. Godsave G. A. E., in *Fourth Symposium (International) on Combustion*, Williams & Wilkins, Baltimore, 1953, pp. 818–830.
64. Chao, B. H., Law, C. K., and T'ien, J. S., in *Twenty-Third Symposium (International) on Combustion*, The Combustion Institute, Pittsburgh, 1990, pp. 523–531.
65. Cheatham, S. and Matalon, M., in *Twenty-Sixth Symposium (International) on Combustion*, The Combustion Institute, Pittsburgh, 1996, pp. 1063–1070.
66. Dietrich, D. L., Dryer, F. L., Haggard, J. B., Nayagam, V., Shaw, B. D., and Williams, F. A., in *Twenty-Sixth Symposium (International) on Combustion*, The Combustion Institute, Pittsburgh, 1996, pp. 1201–1207.
67. Nayagam, V., Haggard, J. B., Colantonia, R. D., Marchese, A. J., Dryer, F. L., Zhang, B. L. and Williams, F. A., *AIAA J.* 36:1369–1378 (1998).
68. Choi, M. Y., Dryer, F. L., and Haggard, J. B., in *Twenty-Third Symposium (International) on Combustion*, The Combustion Institute, Pittsburgh, 1990, pp. 1597–1604.
69. Jackson, G. S. and Avedesian, C. T., *Proc. R. Soc. London* A446:255–276 (1994).
70. Marchese, A. J., Dryer, F. L., and Nayagam, V., *Combust. Flame* 116:432–459 (1999).
71. King, M. K., in *Twenty-Sixth Symposium (International) on Combustion*, The Combustion Institute, Pittsburgh, 1996, pp. 1227–1235.
72. Shaw, B. D., Dryer, F. L., Williams, F. A., and Haggard, J. B., *Acta Astronautica* 17:1195–1202 (1988).
73. Jackson, G. S., Avedesian, C. T., and Yang, J. C., *Int. J. Heat Mass Transfer* 35:2017–2033 (1992).
74. Cho, S. Y., Choi, M. Y., and Dryer, F. L., in *Twenty-Third Symposium (International) on Combustion*, The Combustion Institute, Pittsburgh, 1990, pp. 1611–1617.
75. Yang, J. C., Jackson, G. S., and Avedesian, C. T., in *Twenty-Third Symposium (International) on Combustion*, The Combustion Institute, Pittsburgh, 1990, pp. 1619–1625.
76. Nayagam, V. and Williams, F. A., in *Seventh International Conference on Numerical Combustion*, Society for Industrial and Applied Mathematics, Philadelphia, PA, 1998, p. 46.
77. Dietrich, D. L., Ross, H. D., and T'ien, J. S., AIAA paper 94-0429.
78. Dietrich, D. L., Ross, H. D., Frate, D. T., Tien, J. S., and Shu, Y., in *Proceedings of the Fourth International Microgravity Combustion Workshop*, NASA Conference Publication 10194, 1997, pp. 237–242.
79. Buckmaster, J. D., *Combust. Sci. Technol.* 115:41–68 (1996).
80. Grayson, G. D., Sacksteder, K. R., Ferkul, P., and T'ien, J. S., *Microgravity Sci. Technol.* 7:187–195 (1994).
81. deRis, J. N., in *Twelfth Symposium (International) on Combustion*, The Combustion Institute, Pittsburgh, 1968, pp. 241–252.
82. Delichatsios, M. A., *Combust. Sci. Technol.* 44:257–267 (1986).
83. Olson, S. L., Ferkul, P. V., and Tien, J. S., in *Twenty-Second Symposium (International) on Combustion*, The Combustion Institute, Pittsburgh, 1988, pp. 1213–1222.
84. Rhatigan, J. L., Bedir, H., and T'ien, J. S., *Combust. Flame* 112:231–241 (1998).
85. Olson, S. L., *Combust. Sci. Technol.* 76:233–249 (1991).
86. Ramachandra, P. A., Altenkirch, R. A., Bhattacharjee, S., Tang, L., Sacksteder, K., Wolverton, M. K., *Combust. Flame* 100:71–84 (1995).
87. Bhattacharjee, S., Altenkirch, R. A., and Sacksteder, K., *J. Heat Transfer* 118:181–190 (1996).
88. Honda, L. and Ronney, P. D., *Combust. Sci. Technol.* 133:267–291 (1998).
89. West, J., Tang, L., Altenkirch, R. A., Bhattacharjee, S., Sacksteder, K., Delichatsios, M. A., in *Twenty-Sixth Symposium (International) on Combustion*, The Combustion Institute, Pittsburgh, 1996, pp. 1335–1343.
90. Bhattacharjee, S., Altenkirch, R. A., Worley, R., Tang, L., Bundy, M., Sacksteder, K., Delichatsios, M. A., in *Proceedings of the Fourth International Microgravity Combustion Workshop*, NASA Conference Publication 10194, 1997, pp. 387–392.
91. Olson, S. L., Baum, H. R., Kashiwagi, T., in *Twenty-Seventh (International) Symposium on Combustion*, The Combustion Institute, Pittsburgh, 1998, pp. 2525–2533.
92. Chen, R. H., Mitchell, G. B., Ronney, P. D., in *Twenty-Fourth (International) Symposium on Combustion*, The Combustion Institute, Pittsburgh, 1992, pp. 213–221.
93. Kim, J. S., Williams, F. A., and Ronney, P. D., *J. Fluid Mech.* 327:273–302 (1996).

94. Zik, O. and Moses, E., in *Twenty-Seventh (International) Symposium on Combustion*, The Combustion Institute, Pittsburgh, 1998, pp. 2815–2820.
95. Ross, H. D., *Prog. Energy Combust. Sci.* 20:17–63 (1994).
96. Miller, F. J. and Ross, H. D., in *Twenty-Fourth (International) Symposium on Combustion*, The Combustion Institute, Pittsburgh, 1992, pp. 1703–1711 (1992).
97. Ross, H. D. and Miller, F. J., in *Twenty-Sixth Symposium (International) on Combustion*, The Combustion Institute, Pittsburgh, 1996, pp. 1327–1334 (1996).
98. Schiller, D. N., Ross, H. D., and Sirignano, W. A., *Combust. Sci. Technol.* 118:203–255 (1996).
99. Ronney, P. D., in *Modeling in Combustion Science* (J. D. Buckmaster and T. Takeno, eds.), Lecture Notes In Physics, vol. 449, Springer-Verlag, Berlin, 1995, pp. 3–22.
100. Chin, H. H. and Chang, S. S., AIAA paper 93-2194.
101. Chang, K. C. and Shieh, J. S., *Int. J. Heat Mass Transfer* 38:2611–2621 (1995).
102. Siegel, R. and Howell, J. R., *Thermal Radiation Heat Transfer*, 3rd ed., Hemisphere, Washington, D.C., 1992.
103. Bedir, H., Tien, J. S., and Lee, H. S., *Combust. Theory Modeling* 1:395–404 (1997).
104. Egolfopoulos, F. N. and Law, C. K., *Combust. Flame* 80:7–16 (1990).
105. Vieille, B., Chauveau, C., Chesneau, X., Odeide, A., Gokalp, I., in *Twenty-Sixth Symposium (International) on Combustion*, The Combustion Institute, Pittsburgh, 1996, pp. 1259–1265.
106. Kashiwagi, T., McGrattan, K. B., Olson, S. L., Fujita, O., Kikuchi, M., Ito, K., in *Twenty-Sixth Symposium (International) on Combustion*, The Combustion Institute, Pittsburgh, 1996, pp. 1345–1352.
107. Patnaik, G., Kailasanath, K., and Sinkovits, R. S., in *Twenty-Sixth Symposium (International) on Combustion*, The Combustion Institute, Pittsburgh, 1996, pp. 899–905.
108. Struk, P. M., Dietrich, D. L., and Tien, J. S., *Micrograv. Sci. Technol.* 9:106–116 (1996).
109. Atreya, A., Everest, D. A., Agrawal, S., and Anderson, M. K., in *Proceedings of the Fourth International Microgravity Combustion Workshop*, NASA Conference Publication 10194, 1997, pp. 63–68.
110. Law, C. K., Sung, C. J., and Zhu, D. L., in *Proceedings of the Fourth International Microgravity Combustion Workshop*, NASA Conference Publication 10194, 1997, pp. 69–74.
111. Pfefferle, W. C. and Pfefferle, L. D., *Prog. Energy Combust. Sci.* 12:25–41 (1986).
112. Warnatz, J., in *Twenty-Fourth Symposium (International) on Combustion*, The Combustion Institute, Pittsburgh, 1992, pp. 553–579.
113. Ronney, P. D., *Combust. Flame* 62:120–132 (1985).
114. Egolfopoulos, F. N. and Law, C. K., in *Twenty-Third Symposium (International) on Combustion*, The Combustion Institute, Pittsburgh, 1990, pp. 413–421.
115. Williams, F. A., in *Sixteenth Symposium (International) on Combustion*, The Combustion Institute, Pittsburgh, 1976, pp. 1281–1294.

COMMENTS

H. S. Mukunda, Indian Institute of Science, Bangalore, India. In your presentation, you credited the computational demonstration of the result on the absence of a flammability limit in adiabatic flames to Giovangigli and Smooke [1]. This result was first obtained in 1988 [2]. You might like to amend the citation suitably.

REFERENCES

1. Giovangigli, V. and Smooke, M., *Combust. Sci. Technol.* 87:241 (1992).
2. Lakshmisha, K. N., et al., in *Twenty-Second Symposium (International) on Combustion*, The Combustion Institute, Pittsburgh, 1988, pp. 1573–1578.

Author's Reply. In this earlier paper by the questioner and his collaborators [2], it was shown that the solutions of the unsteady planar one-dimensional adiabatic premixed flame equations do not predict any flammability limit for lean CH_4-O_2-N_2 mixtures—the burning velocity decreases asymptotically to zero as the mixture strength is decreased. In Smooke and Giovangigli (Ref. [1] of the comment), the steady version of these equations was solved for CH_4–air and H_2–air mixtures, and a similar conclusion was reached. Both are important findings, because it is possible in principle that unsteady effects could suppress limits of steady flames or cause limits to occur for mixtures that are flammable as steady flames. Together they show that one must identify loss mechanisms of the appropriate magnitude to explain flammability limits, which was one of the key points of my presentation.

•

J. P. Gore, Purdue University, USA. You seem to have drawn a conclusion based on your time-scale analysis that "radiation is not important at 1 g." For combustion under high-pressure conditions, for fires (large and small), and for all flames as far as high activation energy reaction steps are involved, radiation can be potentially important. Could you please re-examine and clarify your conclusion regarding radiation not being important at 1 g?

Author's Reply. Certainly radiation is an important mechanism of heat transfer in flames even at 1 g—large

industrial furnaces and boilers depend almost entirely on radiative transfer. The same is true of many large accidental fires (e.g., in buildings, over liquid fuel pools). The message I intended to convey was that the radiation transport time scale is longer than the buoyant transport time scale at earth gravity, and thus radiation does not play an important role on local flame structure and extinction conditions at earth gravity compared to the role that buoyant convection plays. Even on the large scale, however, buoyancy is probably a more dominant transport mechanism at 1 g—while a building fire would be very different with buoyancy but no radiation, imagine how different it would be with radiation but no buoyancy!